Biochimica et Biophysica Acta 1798 (2010) 909–927

Contents lists available at ScienceDirect

Biochimica et Biophysica Acta

journal homepage: www.elsevier.com/locate/bbamem

Three unrelated sphingomyelin analogs spontaneously cluster into plasma membrane micrometric domains

D. Tyteca [a,*], L. D'Auria [a], P. Van Der Smissen [a], T. Medts [a], S. Carpentier [a], J.C. Monbaliu [b], P. de Diesbach [a], P.J. Courtoy [a]

[a] CELL Unit, Université catholique de Louvain and de Duve Institute, Brussels, Belgium
[b] CHOM Unit, Université catholique de Louvain, Louvain-la-Neuve, Belgium

ARTICLE INFO

Article history:
Received 21 August 2009
Received in revised form 22 January 2010
Accepted 27 January 2010
Available online 1 February 2010

Keywords:
Sphingomyelin
Micrometric domain
CHO plasma membrane
Erythrocyte
Lateral diffusion
Phase coexistence

ABSTRACT

Micrometric lipid compartmentation at the plasma membrane is disputed. Using live confocal imaging, we found that three unrelated fluorescent sphingomyelin (SM) analogs spontaneously clustered at the outer leaflet into micrometric domains, contrasting with homogeneous labelling by DiIC18 and TMA-DPH. In erythrocytes, these domains were round, randomly distributed, and reversibly coalesced under hypotonicity. BODIPY-SM and -glucosylceramide showed distinct temperature-dependence, in the same ranking as Tm for corresponding natural lipids, indicating phase behaviour. Scanning electron microscopy excluded micrometric surface structural features. In CHO cells, similar surface micrometric patches were produced by either direct BODIPY-SM insertion or intracellular processing from BODIPY-ceramide, ruling out aggregation artefacts. BODIPY-SM surface micrometric patches were refractory to endocytosis block or actin depolymerization and clustered upon cholesterol deprivation, indicating self-clustering at the plasma membrane. BODIPY-SM excimers further suggested clustering in ordered domains. Segregation of BODIPY-SM and -lactosylceramide micrometric domains showed coexistence of distinct phases. Consistent with micrometric domain boundaries, fluorescence recovery after photobleaching (FRAP) revealed restriction of BODIPY-SM lateral diffusion over long-range, but not short-range, contrasting with comparable high mobile fraction of BODIPY-lactosylceramide in both ranges. Controlled perturbations of endogenous SM pool similarly affected BODIPY-SM domain size by confocal imaging and its mobile fraction by FRAP. The latter evidence supports the hypothesis that, as shown for BODIPY-SM, endogenous SM spontaneously clusters at the plasmalemma outer leaflet of living cells into ordered micrometric domains, defined in shape by liquid-phase coexistence and in size by membrane tension and cholesterol. This proposal remains speculative and calls for further investigations.

1. Introduction

Lipids are the most abundant constituents of biological membranes and regulate their fluidity. Among them, sphingolipids (SLs) including sphingomyelin (SM) are not only essential for membrane structure/organization [1], but also play important signalling roles [2]. In the original fluid mosaic model, plasma membrane (PM) lipids were considered to form a homogeneous two-dimensional bilayer, serving as fence to hydrophilic compounds, as gate to small hydrophobic molecules, and as solvent for transmembrane proteins [3]. However, it has become increasingly accepted that some membrane lipids, including SM and cholesterol, spontaneously cluster into discrete "lipid rafts", thereby creating lateral asymmetry [4,5]. Lipid rafts are defined as nanometric heterogeneous membrane domains enriched in cholesterol and SLs bearing saturated alkyl chains, which become closely packed to form together liquid-ordered (L_o) domains [6]. Lipid rafts are operationally defined either as non-ionic detergent-resistant membranes at low temperatures (DRMs), which can be further purified by floatation in density gradients [6,7], or by their sensitivity to cholesterol- or SLs-depleting agents [8]. Nanometric lipid rafts can be visualized by atomic force microscopy [9], by stimulated emission depletion far-field fluorescence nanoscopy [10], or by confocal

Abbreviations: BODIPY, boron dipy*_r_*romethenedifluoride; BODIPY^{505}, BODIPY "green"; BODIPY^{589}, BODIPY "red"; Cer, ceramide; DF-BSA, defatted bovine serum albumin; DiI, dialkylindocarbocyanine; DRMs, detergent-resistant membranes; FB1, fumonisin B1; GlcCer, glucosylceramide; GPMVs, giant PM vesicles; GSL, glycosphingolipid; GUVs, giant unilamellar vesicles; LacCer, lactosylceramide; L_d, liquid-disordered; L_o, liquid-ordered; mβCD, methyl-β-cyclodextrin; mβCD:chol, methyl-β-cyclodextrin:cholesterol; NBD, 7-nitrobenz-2-oxa-1,3-diazol-4-yl; *N*-Rh-PE, 1,2-dioleoyl-sn-glycero-3-phosphoethanolamine-*N*-lissamine rhodamine B sulfonyl; PC, phosphatidylcholine; PM, plasma membrane; S_o, solid-ordered; SL, sphingolipid; SM, sphingomyelin; SMase, sphingomyelinase; Tm, phase transition temperature; TMA-DPH, 1-[4-(trimethylamino) pheny]-6-phenyl-1,3,5-hexatriene

* Corresponding author. CELL Unit, de Duve Institute, Université catholique de Louvain, UCL 75.41, avenue Hippocrate, 75, B-1200 Brussels, Belgium. Tel.: +32 2 764 75 91; fax: +32 2 764 75 43.
E-mail address: donatienne.tyteca@uclouvain.be (D. Tyteca).

0005-2736/$ – see front matter © 2010 Elsevier B.V. All rights reserved.
doi:10.1016/j.bbamem.2010.01.021

microscopy upon cross-linking procedures, such as binding of the pentavalent B subunit of cholera toxin (CTXB) to GM1, a representative SL, or antibody-mediated cross-linking of GPI-linked proteins into caveolae [11]. However, attempts to visualize lipid rafts by confocal microscopy without cross-linking have remained unsuccessful [for reviews, see 12,13]. PM lipid rafts can recruit a variety of proteins that regulate various signalling events [for a review, 14], including at the immunological synapse [15], and may participate in clathrin-independent endocytosis [16]. In yeast, although some PM proteins show mutually exclusive localization, all of them are associated with DRMs at the cell surface, due to the abundance of extremely long chain SLs and the ability of ergosterol to form remarkably resistant microdomains [17]. These observations underline the heterogeneity of rafts.

Whereas a consensus has been reached on a general definition of nanometric rafts [18,19], the concomitant occurrence of micrometric domains at the PM of living cells under physiological conditions is largely debated [20], if not dismissed [21]. In model (but artificial) systems of liposomes or PM-derived structures labelled by mixtures of fluorescent lipid analogs or lipidomimetic dyes, micrometer-large domains can be readily visualized due to partition between L_o- and liquid-disordered (L_d)-phases. Examples include mixing of fluorescent lipid analogs with purified natural lipids or with complex lipidic extracts from cell membranes, followed by formation of giant unilamellar vesicles (GUVs) or supported lipid monolayers [22,23]; or insertion of fluorescent lipids into large plasma membrane vesicles (GPMVs) [24]. About two decades ago, Rodgers and Glaser even reported that labelling of erythrocyte ghosts with L_d-fluorescent glycerophospholipids concentrated into one or two micrometric domains, with distributions depending on the headgroup, but less-defined equivalents were noticed in the living state [25]. Alternatively, formation of lipid domains visible in living cells by fluorescence microscopy often required major alterations in lipid contents. For instance, surface digestion of living erythrocytes by phospholipase C/sphingomyelinase led to the formation of micrometric domains enriched with fluorescent ceramide [26]. Likewise, lowering cholesterol levels induced the formation of visible micrometric domains on several mammalian cell types [27]. It is thus no surprise that the very artificial conditions mostly used so far to evidence micrometric domains led instead to the opposite suggestion, i.e. that the formation of such micrometric lipid membrane domains in untreated living cells is actually prevented, due to interactions with membrane proteins and with the cytoskeleton [24].

However, phase coexistence of micrometric lipid membrane domains has been documented in living cells, in some cases with unquestionable approaches, but in other cases under non-physiological conditions, which left critical readers sceptical on the whole concept. In living erythrocytes, phase coexistence has been evidenced by: (i) Laurdan general polarization (GP) values at 25–35 °C, which allowed to detect lipid order and phases [28]; (ii) phase mapping, which distinguished two types of domains, of either low fluidity, low spacing and high order; or higher fluidity and larger spacing [29]; (iii) FTIR (Fourier transform infrared spectroscopy), which unravelled multiple sharp membrane phase transitions at 4 °C [30]. On living blood platelets, the distribution of the L_o-lipidomimetic synthetic dye DiIC18 becomes inhomogeneous around 24 °C, suggesting lipid phase separation [31,32]. In nucleated cells, micrometric membrane patches with phase separation have also been reported: (i) in CHO cells at 33–34 °C with NBD-SM [27]; (ii) in macrophages with Laurdan GP values at physiological temperatures [33]; and (iii) in fibroblasts with BODIPY-L-*t*-lactosylceramide at 10 °C [34].

Besides imaging and biophysical methods, the existence of domains has also been supported by functional evidence. In their landmark 1987 paper, Yechiel and Edidin studied living fibroblasts after insertion of NBD-phosphatidylcholine (PC) and reported that the comparison of lateral diffusion parameters derived from fluorescence recovery after photobleaching (FRAP) of increasing field sizes implied the existence of micrometer-scale domains [35]. Since the organization of membrane domains can alternatively be probed using fluorescent proteins, combined confocal and FRAP analyses of polarized epithelial cells transfected with expression vectors for fluorescent protein, engineered to partition or not with rafts, revealed large domains at the apical PM, much larger than expected from the usual "small" rafts [36]. However, with a few exceptions listed above, large lipid domains have not been detected in untreated cells. Furthermore, the relevance of micrometric domains resulting from cross-linking in living cells [37], as well as their genuine existence as opposed to anatomical features such as folds, ruffles, microvilli and filopodia [38,39] have been questioned.

Yet, elucidating the organization of lipids at the PM under physiological conditions is of paramount importance. Indeed, "stable" lipid phases may determine lipid mobility and duration of their interactions with membrane proteins, and therefore deeply affect membrane functionality as a whole. We here re-examined whether micrometric SM domains could naturally occur at the PM of the smooth-membraned erythrocytes and on the well-characterized CHO cell line, using fluorescent analogs analyzed by confocal imaging and FRAP. Four reasons guided our main choice on BODIPY^{505}-SM. Firstly, BODIPY^{505}-SM shows a very high quantum yield and good photostability. Secondly, SM is the major SL in human erythrocytes and in most other mammalian cells, and it plays important structural and signalling roles [2]. Thirdly, SM is restricted to the outer PM leaflet, where various fluorescent analogs can be readily inserted and analyzed without flip-flop and diffusion into the cytosol, allowing to study their clustering by confocal microscopy and their dynamics by FRAP. Alternatively, BODIPY-SM can be generated inside the cell upon enzymatic conversion from BODIPY-ceramide, an invaluable approach to rule out primary aggregation artefacts. Fourthly, SM bears long saturated acyl chains, thus forming gel-like phases by ordered lipid: lipid interactions, which can be probed by spectral shift of emitted light at high BODIPY^{505}-SM concentration (excimers).

We here provide several lines of evidence showing that BODIPY^{505}-SM and two other SM analogs spontaneously cluster at the outer PM leaflet of living cells into ordered micrometric domains, defined in shape by liquid-phase coexistence and in size by membrane tension and cholesterol, but without requiring cortical microfilaments. This general conclusion is based on (i) the combination of confocal imaging at various temperatures and in several cell types as well as multiple conditions with lateral diffusion measurements by FRAP for three fluorescent SM analogs; (ii) careful exclusion of a variety of possible artefacts; and (iii) the study of the relation with endogenous SM, by its selective depletion and repletion. To the extent that these analogs are reasonable qualitative surrogates of endogenous SM, the latter line of evidence supports the hypothesis that SM may naturally form micrometric PM domains, but this proposal needs to be further and thoroughly tested.

2. Materials and methods

2.1. Commercial lipids and reagents

1,2-Dioleoyl-sn-glycero-3-phosphoethanolamine-*N*-(lissamine rhodamine B sulfonyl) (*N*-Rh-PE), lyso-sphingomyelin, glucosyl-β-sphingosine and lactosyl-β1-sphingosine were from Avanti polar lipids. Ceramides, sphingomyelins, GM3 and glucocerebrosides were from Matreya. D-*erythro N*-(4,4-difluoro-5,7-dimethyl-4-bora-3a,4a-diaza-*s*-indacene-3-pentanoyl)sphingosyl1-β-D-lactoside (BODIPY-D-*e*-LacCer) was a kind gift of Professor D. Pagano. All other fluorescent lipids, Amplex Red Cholesterol assay kit, *N*-hydroxysuccinimidyl ester of 4,4-difluoro-5,7-dimethyl-4-bora-3a,4a-diaza-*s*-indacene-3-pentanoic acid (BODIPY^{505}-fatty acid), and off 6-(((4-(4,4-difluoro-5-(2-thienyl)-4-bora-3a,4a-diaza-*s*-indacene-3-yl)phenoxy)acetyl)amino)hexanoic acid (BODIPY^{589}-fatty acid) and Vybrant DiI (DiIC18) were from Invitrogen. TMA-DPH, poly-L-lysine (70–

150 kDa), methyl-beta-cyclodextrin (mβCD), mβCD:cholesterol complex (6:1 molar ratio), fumonisin B1 (FB1), *Bacillus cereus* sphingomyelinase (SMase), defatted bovine serum albumin (DF-BSA), NaN_3 and 2-deoxy-D-glucose were from Sigma-Aldrich. Latrunculin B was from Merck.

2.2. Synthesis and analysis of fluorescent lipids

SM, GlcCer and D-*e*-LacCer were conjugated to BODIPY^{505} (or BODIPY^{589}) by *N*-acylation [40] of lyso-sphingomyelin, glucosyl-β-sphingosine and lactosyl-β1-sphingosine respectively, using the *N*-hydroxysuccinimidyl ester of corresponding BODIPY-fatty acids. The two reagents were mixed in acetonitrile solvent in the presence of diisopropylethylamine (Sigma-Aldrich) under argon atmosphere and the reaction was allowed to develop at 37 °C during 20–30 h. Products were purified by preparative thin (1 mm) layer chromatography (TLC) in silica gel 60 F_{254} (Merck, Amsterdam) using chloroform: methanol (9:1, v/v). After scraping, TLC bands were extracted by filtration using elution by ethyl acetate:isopropanol (8:2, v/v). After evaporation, final products were dissolved in ethanol. The identity and purity of the products were confirmed by ^{2}H-NMR and mass spectrometry. Lipid concentration was determined using a Perkin-Elmer LS-30 spectrofluorimeter by reference to standards. To study BODIPY-ceramide to -SM bioconversion, total cell lipids were extracted [41] and analyzed by TLC in chloroform:methanol:15 mM $CaCl_2$ (65:35:8; v/v/v) [42].

2.3. Erythrocyte isolation, immobilization on poly-L-lysine and labelling with fluorescent probes

Human erythrocytes were collected from two healthy donors by veinopuncture in dry EDTA tubes and 100 µl were diluted 1:10 in Hank's Buffered Salt Solution (HBSS; 137.9 mM NaCl, 10 mM HEPES, pH 7.2, 5.5 mM D-glucose, 5.3 mM KCl, 1.26 mM $CaCl_2$, 0.49 mM $MgCl_2$, 0.44 mM KH_2PO_4, 0.41 mM $MgSO_4$, 0.34 mM Na_2HPO_4), except stated otherwise, and centrifuged at 1300 rpm (133×*g*) for 2 min in a Jouan centrifuge. The pellet was washed again by suspension in 1 ml HBSS, centrifugation as above and resuspension. Twenty µl of the resuspension were diluted 1:50 in HBSS and allowed to bind at the final temperature for 7 min to a 1.33-cm^2 glass coverslip precoated for maximum 5 min with 0.01% poly-L-lysine (w/v). After 3 washes with HBSS, coverslip-bound erythrocytes were adapted to the final temperature for 2–10 min, then labelled with 1 µM BODIPY^{505}-SM or -GlcCer or 4.5 µM TMA-DPH, all in HBSS containing DF-BSA (1:1 molar ratio) at 4 °C for 30 min or at 20 °C, 30 °C or 37 °C for 15 min, and examined after 5 rapid washes (except for TMA-DPH). Coverslips were then placed bottom-up into a Lab-Tek chamber so that the free upper cell surface (not in contact with poly-L-lysine) was directly viewed by the objective at the controlled temperature. Alternatively, since DiIC18 aggregated at 20 °C, erythrocytes were incubated with 5 µM Vybrant DiI (DiIC18) in HBSS containing 1 mg/ml DF-BSA at 37 °C for 15 min, then washed in HBSS at 20 °C or 37 °C and examined at the same temperature.

2.4. Scanning electron microscopy

Adherent erythrocytes (labelled or not with BODIPY^{505}-SM) were extensively washed with HBSS, rinsed twice in 0.14 M cacodylate buffer, pH 7.4, then fixed at room temperature with carefully increasing glutaraldehyde concentrations [Fluka-Sigma; 0.1, 0.5 and 1% (v/v) in 0.1 M cacodylate buffer for 30 min each], followed by 2% glutaraldehyde at 4 °C overnight. The next day, samples were extensively washed in 0.1 M cacodylate buffer and post-fixed with 1% (w/v) OsO_4 at 4 °C for 2 h. Samples were then dehydrated in graded ethanol series and critical-point dried (CPD 0.20, Balzers Union, Liechtenstein). A 10-nm gold film was sputter-coated, and specimens were observed in a CM12 electron microscope at 80 kV with the use of the secondary electron detector (Philips, Eindhoven, Netherlands).

2.5. Cell culture, transfection and pharmacological treatments

CHO and HeLa cells were propagated in DMEM/F-12 medium (Gibco-Invitrogen; hereafter referred to as medium) supplemented by 10% fetal calf serum (FCS) and antibiotics (10 µg/ml streptomycin and 66 µg/ml penicillin; all from Gibco-Invitrogen). J774 were propagated as previously described [43]. For experiments, cells were seeded at 20,000/cm^2 and grown till ~90% confluency (2 days) on Lab-Tek chambers (Nunc, Roskilde, Denmark; live cell imaging and FRAP) or Petri dishes (biochemical experiments). CHO cells were transfected with actin-YFP or GPI-GFP plasmids [36] using lipofectamine at 37 °C for 5 h (0.25 µg DNA and 0.5 µl lipofectamine/cm^2), after which cells were transferred into fresh medium supplemented by 10% FCS without antibiotics for 24 h. Control experiments indicated that lipofectamine treatment one day before confocal imaging had no detectable effect on BODIPY-SM micrometric domains.

When appropriate, before surface labelling, cells were preincubated at 37 °C with 25 or 50 nM latrunculin B for 30 min, 0.1 U/ml SMase for 30 min, or 5 mM mβCD for 3 h, all in medium; or 0.4 mM mβCD:Chol for 2 h or 30 µM FB1 for 48 h, both in serum-containing medium. SMase treatment led to ~50% total SM depletion, which was reversible upon incubation with serum-containing medium at 37 °C for 4 h. FB1-treatment led to ~40% total SM depletion (Supplementary Table 2). Some FB1-treated cells were selectively replenished with 20 µM C_8-ceramide, C_6-SM or GM3 at 4 °C for 30 min. None of these treatments caused detectable toxicity, as shown by lack of significant release of lactate dehydrogenase in the medium. To block endocytosis, cells were either ATP-depleted by incubation at 37 °C for 5 min in glucose-free medium supplemented by 10 mM NaN_3 and 50 mM 2-deoxy-D-glucose, or K^+-depleted by incubation in hypotonic medium at 37 °C for 5 min, then in K^+-free medium for 30 min [44]. Live cell imaging and FRAP analysis were performed in the continued presence of latrunculin B, ATP- or K^+-depleting medium.

2.6. Cell surface labelling with fluorescent probes

Most experiments were carried out with BODIPY^{505}-SM (also referred to for simplicity as BODIPY-SM) in CHO cells. Unless using the dialysis procedure (see below), dried lipid analogs were dissolved in absolute ethanol and mixed with medium enriched with equimolar DF-BSA and 30 mM HEPES under vigorous vortexing, then cleared of aggregates by centrifugation at 14,000×*g* for 5 min. Unless otherwise stated, for surface labelling, cells were transferred into ice-cold medium for 10 min, then incubated at 4 °C for 30 min with the following lipid:BSA complexes at <0.5% final ethanol concentration: 1 µM BODIPY^{505}-SLs (-SM, -D-*e*-LacCer) (except 5 µM BODIPY^{505}-SM for excimer studies), 1.5 µM BODIPY^{589}-SM, 3 µM BODIPY^{589}-GlcCer, 5 µM NBD-SM or 5 µM *N*-Rh-PE. Alternatively, to further exclude insertion as aggregates, BODIPY-SM was incorporated into cells after dialysis and ultracentrifugation as described [45]. Briefly, BODIPY-SM was dissolved in ethanol and mixed with equimolar BSA in medium and the complex was dialyzed overnight at 4 °C against medium (MW cut-off 12–14 kDa; Spectra/Por molecular porous membrane) and spun at 100,000×*g* for 20 min. The concentration of BODIPY-SM:BSA complexes in the supernatant was determined by fluorescence with reference to a known standard. For bioconversion experiments, CHO cells were surface-labelled with 5 µM BODIPY^{505}-ceramide in ice-cold culture medium for 30 min as above, rapidly washed and incubated at 37 °C to allow for intracellular processing into BODIPY^{505}-SM. After cell surface labelling or further bioconversion, cells were washed 5 times with serum-free medium at 4 °C, then analyzed by confocal

microscopy or FRAP. Level of insertion and integrity of probes were evaluated, as reported at Supplementary Table 1.

2.7. Live cell imaging

All morphological studies were performed by vital imaging using Plan-Apochromat 63×/1.4 oil immersion objectives, except for TMA-DPH (C-Apochromat 63×/1.2 water objective). After labelling with fluorescent lipids, cells were washed, transferred to medium adjusted to the observation temperature set at 10 °C, 20 °C, 30 °C or 37 °C as indicated, and immediately analyzed by confocal microscopy at the same temperature. Alternatively, CHO cells were submitted to extensive surface back-exchange at 4 °C with 5% BSA (w/v; 3 rounds of 10 min each) prior to examination. Imaging was performed with a Zeiss LSM510 confocal microscope set at 20 °C, 30 °C or 37 °C (XL/LSM incubator, Zeiss), or with a Bio-Rad MRC1024/Zeiss Axiovert M135 confocal microscope equipped with a cooling/warming stage adjusted to reach an effective temperature of ~10 °C in the observation chamber (Lauda Ecoline Staredition RE106; Lauda-Königshofen, Germany). We verified that after labelling at 4 °C followed by reincubation at 10 °C for 20 min, <3% of the total pool of BODIPY^{505}-SM acquired resistance to surface back-exchange at 4 °C, confirming the low-temperature endocytosis block. Fields were generally recorded at the bottom (flat) PM to minimize surface anatomical features and to avoid saturation of the lateral PM labelling. Intensity profiles were recorded along paths indicated in orange. For BODIPY^{505}-SLs (-SM, -GlcCer and -D-*e*-LacCer), images were generally recorded at 0.3–2% laser power. BODIPY^{589}-SLs and NBD-SM were respectively viewed at ~30-fold and ~5-fold higher laser power to compensate for lower signal, which was due to the combination of less efficient PM insertion, lower quantum yield and/or faster photobleaching. For double labelling, data were sequentially acquired in the green then in the red channel. For excimer studies, cells were excited at 488 nm and images were simultaneously acquired in both green and red channels. For Vybrant DiI, images were acquired in the red channel at ~5% laser power. For TMA-DPH imaging, two-photon microscopy was performed with a Zeiss LSM510 microscope using excitation at 690–725 nm with ~2% laser power and emission with a 390–465 nm band-pass.

2.8. Fluorescence recovery after photobleaching (FRAP)

FRAP analyses were carried out at 30 °C by setting to this temperature the observation chamber in the MRC 1024/Axiovert M135 confocal microscope or the XL/LSM incubator of the LSM510 META confocal microscope. Cells were examined using Plan-Apochromat 63×/1.4 oil immersion objectives. After selection of flat cells under low illumination, 5- or 20-μm^2-square regions of interest (ROI) were defined (~0.5–2% of the cell surface). After recording of initial intensity (fluorescence before bleaching, I_i), the ROI was briefly photobleached to a minimal residual fluorescence intensity (I_{bleach}; ~10–20% of I_i). Fluorescence recovery with time (I_t) was recorded for 450 s after return to low laser illumination. ROI that had moved during this interval were excluded (<10%). Values were calculated as $(I_t - I_{bleach}) / (I_i - I_{bleach})$ and fitted to a single exponential to extrapolate the mobile fraction at infinite time of recovery (in %). Control experiments for BODIPY^{505}-SM using the Zeiss LSM510 confocal microscope showed undistinguishable recovery, irrespective of photobleaching squares or disks of identical area.

2.9. Statistical analyses

Statistical significance of comparisons was tested using Student's *t* test, using GraphPad Instat programs (GraphPad Software Inc., San Diego).

3. Results

3.1. Experimental strategy: selection of membrane lipid probes and cell models

In this study, sphingomyelin (SM) was selected as a major constituent of the outer PM leaflet, with known preference for L_o-domains. We first probed its PM organization in living cells, using insertion of three fluorescent analogs, generated by grafting well-established fluorophores at the fatty acid alkyl tail: BODIPY^{505} (i.e. "green") and BODIPY^{589} (i.e. "red") derivatives (BODIPY: boron dipy*_r_*romethenedifluoride) and the more photolabile NBD (7-nitrobenz-2-oxa-1,3-diazol-4-yl) [46,47]. Structures are shown in Supplementary Fig. 1. Fluorescent SM analogs were mixed with equimolar DF-BSA as carrier and cleaned of aggregates by centrifugation. Similar results were obtained using a more elaborate procedure involving extensive dialysis and ultracentrifugation (data not shown). As first-choice, we used BODIPY^{505} (λexc 505 nm, green emission) for its high quantum yield, efficient PM insertion and extraction by "back-exchange" with empty BSA, and based on its validation as a qualitative tracer of lipid raft organization [8] and membrane endocytosis [34,48] (see also Discussion). Unless stated otherwise, BODIPY-SM will refer to BODIPY^{505}-SM. BODIPY^{505}-SM compartmentation in the PM could be studied at trace levels in comparison with endogenous SM (Supplementary Table 1). Linearly increasing the concentration of BODIPY^{505}-SM in the medium resulted in proportional increase of its PM content and did not affect its FRAP parameters (data not shown). For double-labelling studies, we synthesized BODIPY^{589}-SM (λexc 589 nm, red emission), because its spectral properties provide clear-cut resolution from BODIPY^{505}. We finally compared a glycosylphosphatidylinositol-anchored protein [GL-GPI-GFP; 36] as another, totally unrelated, reporter of outer leaflet L_o-phases, with the GFP fluorophore standing out the bilayer.

Because the high hemoglobin concentration of erythrocytes generates a strong light filter, lipid domains have been earlier studied in erythrocyte ghosts, which raised doubts as to relevance to living cells. Therefore, we first decided to adapt confocal imaging to the upper free surface of BODIPY-SM-labelled, living human erythrocytes, which offer four major advantages. Firstly, these cells are the most easily accessible ones, show very high homogeneity (since abnormal erythrocytes are rapidly destroyed in the body) and are particularly robust. Secondly, their PM is expected to be featureless at the micrometric level, as we confirmed in our experimental conditions by scanning electron microscopy of untreated erythrocytes, and it remained so after BODIPY-SM-labelling (see Fig. 2E–H). Thirdly, their lipid composition at the outer and inner leaflets is well-documented [30,49]. Fourthly, erythrocytes do not metabolize PM lipids and are endocytosis-defective, thus can be studied at various temperatures without internalization of surface lipid analogs. The latter property is of particular importance for the purpose of this study, since critical phase behaviour was demonstrated in GPMVs [50].

We next extended our study to three other membrane lipid probes, namely (i) BODIPY^{505}-glucosylceramide (GlcCer), as an analog of another SL which exhibits a much higher melting temperature (Tm) than SM [51,52]; (ii) 1-[4-(trimethylamino)pheny]-6-phenyl-1,3,5-hexatriene (TMA-DPH), commonly accepted as a bulk membrane tracer [53,54]; and (iii) the L_o-lipidomimetic dye, dialkylindocarbocyanine DiIC18, which stands among the most widely used fluorescent membrane probes to characterize membrane lateral organization in erythrocytes, blood platelets and nucleated cells [26,27,31,32], because of its brightness, photostability and availability with a variety of hydrocarbon chains [55].

To test for the relevance of micrometric domains in nucleated cells, we further analyzed CHO cells, a paradigmatic cell line which can be easily transfected and is available with a variety of defective mutants for future studies [56]. Except otherwise specified, confocal sections were recorded at the bottom (i.e. "flat") PM, to minimize cell surface

projecting features. In addition, numerous experiments were performed to exclude membrane extensions, including double-labelling experiments of BODIPY-SM with actin microfilaments and with BODIPY^{589}-D-*e*-LacCer, and endocytosis, including ATP- and K^+-depletion. Confirmatory experiments were performed using J774 macrophages, HeLa cells (see Supplementary Fig. 3) and several other cell types (data not shown).

3.2. In living erythrocytes, BODIPY^{505}-SM and -GlcCer formed (sub)micrometric patches; these were controlled by temperature and membrane tension

As shown by Fig. 1A, left, examination of the free surface of freshly isolated erythrocytes labelled with 1 μM BODIPY^{505}-SM:BSA complexes revealed several, round micrometric patches (0.5–1 μm in diameter), whatever the temperature of examination between 10 °C and 37 °C. These patches were sharply defined and exhibited a much brighter homogenous fluorescence than the rest of the membrane viewed "en face" (>8-fold enrichment, see line intensity profile at upper Fig. 1B). The average number of BODIPY^{505}-SM patches varied significantly with the temperature, from ~4 per erythrocyte free surface at 10 °C, to a maximum of 12 ± 2 at 20 °C, then declining back to ~5 at 30 °C and 37 °C (mean ± SEM; $n = 4$ independent experiments with 5–75 erythrocytes each; Fig. 1C, upper panel, open circles). Their cumulative fractional area varied in parallel, covering up to 7 ± 0% of the erythrocyte hemi-surface at 20 °C but only 4–5% at the other temperatures (mean ± SEM; $n = 12$–39, pooled from 3 independent experiments; Fig. 1C, lower panel, open circles). BODIPY^{505}-SM patches were randomly distributed and did not vanish upon actin depolymerization by latrunculin B (data not shown). Upon swelling in mildly hypotonic medium, they coalesced into fewer, larger, centrally located but still round patches (Fig. 1D,a). Reincubation in normotonic medium caused rapid fragmentation of large patches back to the original size (Fig. 1D,b).

Since erythrocytes also contain glycosphingolipids (GSLs) [57], which generally exhibit a much higher melting temperature than SM [51,52], we further tested whether the BODIPY^{505}-GlcCer analog could also form micrometric patches on erythrocytes and whether their number and area would steadily increase with the temperature, up to the physiological one. As predicted, very few or no micrometric patch could be detected at or below 20 °C, but these were constantly observed at 30 °C and largely increased in number and cumulative fractional area at 37 °C (Fig. 1A,e–h). Line intensity profiles at 37 °C showed similar enrichment for BODIPY^{505}-GlcCer as for BODIPY^{505}-SM patches (Fig. 1B, compare lower with upper panel). The distinct effect of temperature on BODIPY^{505}-GlcCer (filled circles) as compared with BODIPY^{505}-SM (open circles) is quantified in Fig. 1C.

Taken together, these data revealed that BODIPY^{505}-SM and BODIPY^{505}-GlcCer spontaneously cluster at the erythrocyte PM into round "domains", presumably to minimize free energy at their boundary, with a size controlled by membrane tension. The modulation by temperature of the number and surface of BODIPY-sphingolipid "domains" further pointed to a role for lipid phase behaviour for their formation and maintenance.

3.3. In contrast to BODIPY^{505}-SM and -GlcCer, DiIC18 and TMA-DPH did not form (sub)micrometric patches in living erythrocytes

In view of the controversy on the very existence of micrometric domains in living cells using labelling by fluorescent lipid analogs, and to tentatively establish a link with their structural/spectral properties, we also evaluated the organization of DiIC18, which preferentially partitions into L_o-domains and can be used to characterize membrane lateral organization in living cells [26,30–32]. Of note, distribution of this probe was reported to be homogeneous in erythrocytes and to be inhomogeneous in platelets only at low temperature [26,30,32]. Since the high lipophilic nature of DiI has been proposed as an obstacle to uniform cellular labelling, we used Vybrant DiI solution to label the erythrocyte membrane. At 20 °C or below, this solution aggregated and yielded low surface labelling intensity. To circumvent this problem, erythrocytes were labelled at 37 °C, washed, then analyzed at this temperature or transferred to 20 °C. In good agreement with the literature [26,30], we did not observe DiIC18 micrometric patches on erythrocytes, neither at 20 °C nor at 37 °C (Fig. 2A,B). In search of an additional negative control for micrometric membrane patches produced by BODIPY^{505}-SM, we looked at TMA-DPH as a "bulk" membrane tracer [53,54]. As shown in Fig. 2C,D, TMA-DPH was not able to induce the formation of micrometric patches, neither at 20 °C nor at 37 °C. These data revealed that, in contrast to BODIPY^{505}-SM and BODIPY^{505}-GlcCer, DiIC18 and TMA-DPH do not cluster at the erythrocyte PM into round "domains".

3.4. BODIPY-SM and -GlcCer (sub)micrometric patches on erythrocytes did not reflect surface structural features

Because erythrocytes can exhibit under artificial conditions structural features such as spicules, particularly upon incorporation of, and deformation by, exogenous amphiphiles [58], we analyzed the surface of adherent erythrocytes by high-resolution scanning electron microscopy, first without any labelling (to verify the preservation of their smooth membrane under our control conditions), then after incubation with BODIPY^{505}-SM resulting into micrometric patches labelling (to exclude induction of corresponding artificial surface features). Untreated adherent erythrocytes uniformly showed a smooth surface, except for the irregular occurrence of very small (nanometric) bulges, considered as preparation artefacts. Since variable stretching of erythrocytes on poly-L-lysine-coated glass could lead to differences in shape and projected size as well as membrane tension, even at the analyzed free surface, scanning electron microscopy was performed both on cell clusters (with the usual ~7.5 μm average diameter; Fig. 2E) and on individual erythrocytes in closer contact with poly-L-lysine-coated coverslips (clearly appearing more stretched and occupying a larger area of the coverslip: ~8.5 μm in diameter; Fig. 2F). Importantly, size and stretching differences affected neither the erythrocyte flat and smooth surface, nor the formation of BODIPY^{505}-SM patches (Fig. 2G′,H′). As a critical control, insertion of BODIPY^{505}-SM into the erythrocyte membrane did not affect morphological characteristics of erythrocytes, whose surface remained free of spicules and protrusions (Fig. 2E–H). The flat scanning electron microscopic appearance of BODIPY-SM-labelled erythrocytes demonstrates that BODIPY-SM patches do not reflect its enrichment into spicules or any other significant surface feature.

3.5. In CHO cells, three fluorescent SM analogs labelled similar PM micrometric patches at 37 °C

Since erythrocytes are very special cells, we next turned our attention to the nucleated CHO cells. To prevent endocytosis, cells were first surface-labelled with BODIPY^{505}-SM:BSA complexes at 4 °C, washed and further viewed by confocal microscopy shortly after transfer to 37 °C (Fig. 3). In addition, to avoid projecting structural features such as ruffles and filopodia, images were preferentially recorded at the bottom (flat) surface. As in erythrocytes, BODIPY^{505}-SM spontaneously clustered on CHO cells into micrometric patches (Fig. 3A,B). If cells were kept at 4 °C, surface back-exchange with empty BSA led to complete disappearance of both patchy and interpatchy labelling, confirming exclusive localization at the PM, not in nearby endocytic structures (data not shown). In CHO cells, BODIPY-SM micrometric patches showed at least ~3-fold enrichment over the rest of the PM (Fig. 3B′), were more heterogeneous in size and shape than in erythrocytes and frequently showed linear alignments, as could be expected from surface restriction due to cortical actin

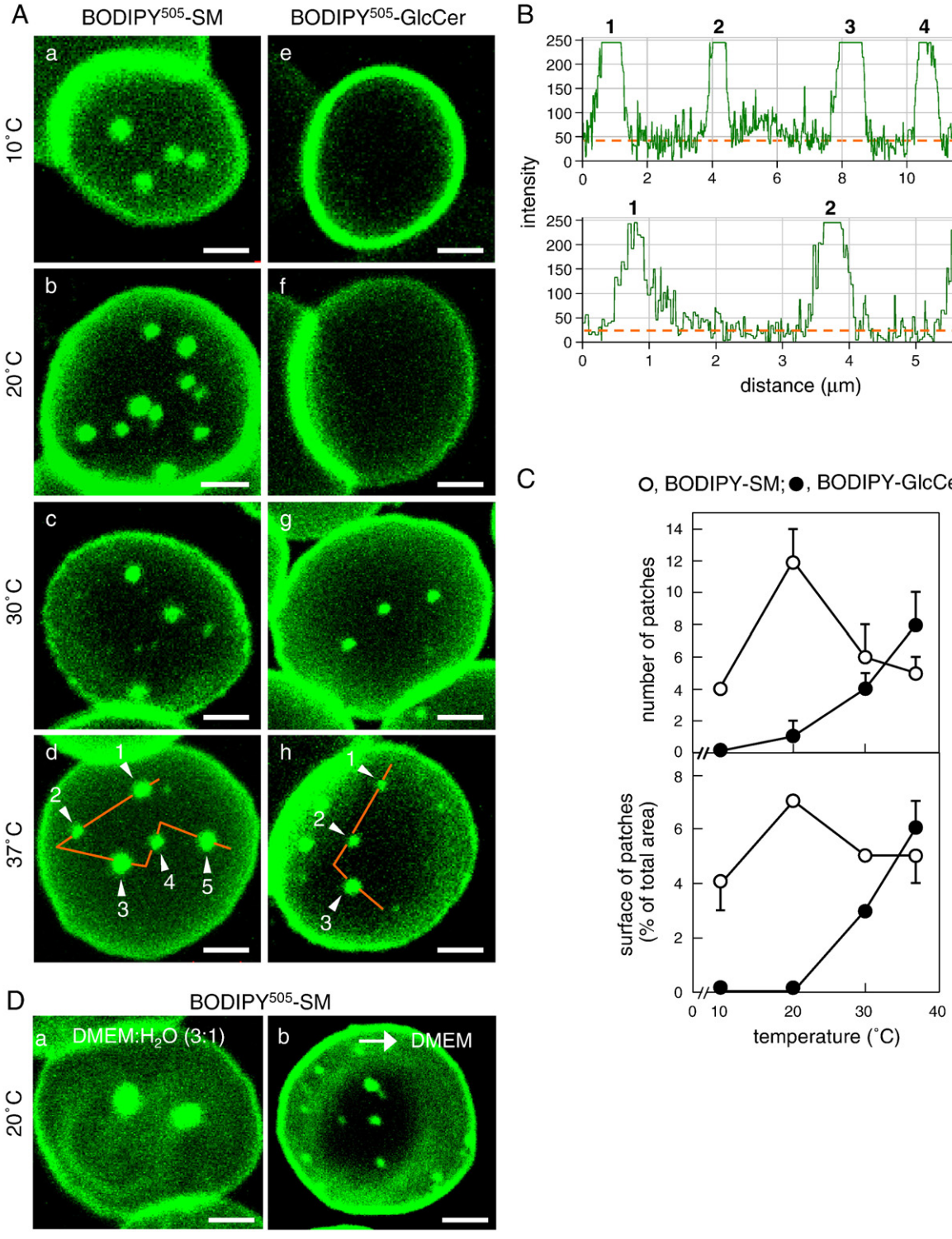

Fig. 1. In living erythrocytes, BODIPY^{505}-SM and -GlcCer spontaneously label (sub)micrometric patches. (A) Confocal imaging. Freshly isolated erythrocytes were washed in HBSS and immobilized on poly-L-lysine-coated coverslips, labelled with BODIPY^{505}-SM (a–d) or -GlcCer (e–h) at the indicated temperatures, then washed. Coverslips were placed upside-down (i.e. with the free erythrocyte surface close to the microscope objective) and examined at the same temperature as for labelling. Note well-defined patches for both tracers at physiological temperature. (B) Fluorescence enrichment. Intensity profiles were recorded at 37 °C along the paths indicated by the continuous orange lines at panel A,d (upper trace) and h (lower trace). Numbers refer to the indicated patches. Note that BODIPY^{505}-SM and -GlcCer-labelled patches are uniformly >8-fold brighter than the rest of the PM (orange dotted line). (C) Morphometry: effect of temperature. Upper panel, number of discrete patches labelled by BODIPY^{505}-SM (open symbols) or -GlcCer (filled symbols) per hemi-cell surface at the indicated temperatures; lower panel, cumulative labelled area as % of analyzed surface (means ± SEM of 3–4 independent experiments, except at 10 °C, 1 experiment, each with 5–75 cells for numbering and 12–39 cells for surface area). Notice different temperature optima, in relation of Tm values of the corresponding endogenous lipids. (D) Effect of membrane tension on the fusion and fission of BODIPY^{505}-SM patches. Erythrocytes were labelled with BODIPY^{505}-SM at 20 °C in normotonic medium as in panel A,b, washed and examined at the same temperature after transfer into moderately hypotonic medium (a) or further return to normotonic medium (b). Notice that increased tension due to hypotonic medium induces fusion/coalescence of BODIPY^{505}-SM into two large central patches, with secondary fission upon return to normal membrane tension. All scale bars, 2 μm.

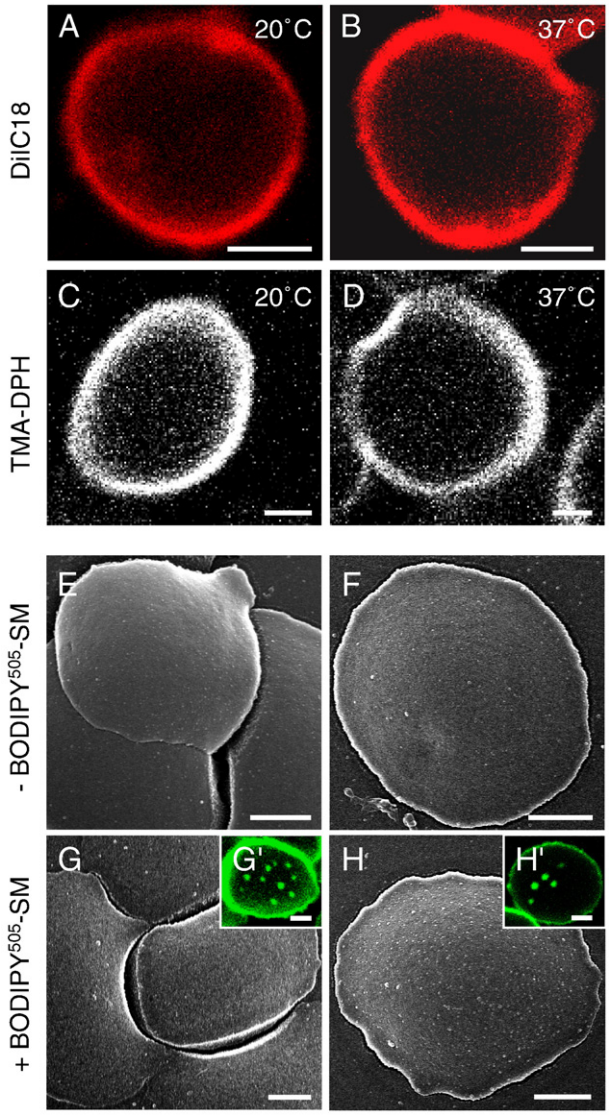

Fig. 2. (Sub)micrometric BODIPY^{505}-SM patches of living erythrocytes do not reflect anatomical surface features. Freshly isolated erythrocytes were immobilized on poly-L-lysine and examined after labelling with DiIC18 (A,B) or BODIPY^{505}-SM (G′,H′) for confocal imaging, or with TMA-DPH for two-photon microscopy (C,D); or processed by scanning electron microscopy without (E,F) or after BODIPY^{505}-SM labelling as above, for smooth-membrane control (G,H). (A–D) The lipidomimetic dyes DiIC18 and TMA-DPH do not form (sub)micrometric patches. (A,B) Erythrocytes were labelled with Vybrant DiI (DiIC18) at 37 °C, washed, and transferred to fresh medium at 20 °C (A) or 37 °C (B) and immediately examined at the same temperature by confocal microscopy. (C,D) Erythrocytes were labelled with TMA-DPH at 20 °C (C) or 37 °C (D) and directly examined. It is clear that none of the lipidomimetic dyes forms detectable patches on erythrocyte membranes viewed "en face", even at the lower spatial resolution of multiphoton microscopy required for TMA-DPH imaging. (E–H) Scanning electron microscopy. (Sub)micrometric BODIPY^{505}-SM patches do not reflect anatomical structures of the erythrocyte membrane. Erythrocytes were immobilized on poly-L-lysine to form small clusters (E,G) or individual cells (F,H), which could spread more extensively at the expense of increased membrane tension. No anatomical (sub) micrometric feature can be detected in relaxed (E) or tense erythrocyte membranes (F). Labelling with BODIPY^{505}-SM as in Fig. 1A,c does not detectably alter the smooth PM (G,H). All scale bars, 2 μm.

(addressed below by Fig. 7), or from differential dynamics due to preferential sites of endocytosis and exocytosis in nucleated cells [59]. Similar brilliant micrometric patches were observed at the upper CHO cell surface, clearly distinct from ruffles and filopodia (Supplementary Fig. 2), and at the bottom surface of J774 macrophages and HeLa cells (Supplementary Fig. 3) and in all other cell types we looked at, indicating that BODIPY^{505}-SM micrometric patches were not dependent on a particular nucleated cell line.

Upon closer look at inter-patchy labelling, we noticed locally decreased fluorescence intensities indicating local depletion, complementary to the local enrichment described above (arrows in Fig. 3B and B′), and suggesting coexistence of adjacent, biochemically distinct (i.e. enriched *vs* depleted) micrometric "domains". When surface-labelled CHO cells were allowed to internalize BODIPY-SM at 37 °C for 10 min, comparison of superficial and intracellular confocal sections also revealed clearly distinct patterns at the cell surface, in the peripheral and in the central cytoplasm. The cell surface labelling pattern has already been described in detail. Peripheral cytoplasmic labelling revealed multiple small, randomly distributed dots and tubules (Fig. 3C), with a low fluorescence intensity emerging over a negligible background (Fig. 3C′), indicating rapid transit across early endosomes. As to the central cytoplasmic labelling, the crowded brilliant structures clustered around one pole of the nucleus (Fig. 3C, see close to *N*) were interpreted as indicating the slowly recycling compartment, based on our unpublished observations. To further exclude that micrometric patches were reflecting the extremely fast recycling peripheral endosomes evidenced by Hao and Maxfield [60], CHO cells were submitted to K^+- or ATP-depletion. Whereas these procedures effectively arrested endocytosis (see below, Fig. 9B′,C′), surface membrane patches were still observed (Fig. 9B,C). Taken together, these observations indicated that spontaneous clustering of BODIPY^{505}-SM occurred at the cell surface.

To exclude that formation of BODIPY^{505}-SM micrometric patches was due to this particular fluorophore, we next compared labelling with two other derivatives: NBD- and BODIPY^{589}-SM (Fig. 4A,B). Both decorated similar cell surface patches and the latter revealed perfect co-localization with BODIPY^{505}-SM in double labelling, as evident in the merged images (Fig. 4C–E). The rapid photobleaching of NBD-SM did not allow to perform a similar double-labelling experiment with BODIPY^{589}-SM. Thus, insertion of three SM analogs, each bearing a structurally different fluorophore (Supplementary Fig. 1), led to the spontaneous formation of similar, if not identical, micrometric patches at the PM of CHO cells at 37 °C.

3.6. BODIPY-SM micrometric PM patches did not reflect BODIPY^{505}-SM aggregation

To next rule out preferential cell surface labelling by BODIPY^{505}-SM aggregates, we used an alternative, more elaborate procedure that included extensive dialysis and ultracentrifugation before incorporation into the PM [45; see Materials and methods]: this approach yielded undistinguishable results (data not shown). A more sophisticated approach than direct surface labelling, entirely conducted at 37 °C, exploited the biosynthetic conversion of the membrane-permeant precursor, BODIPY^{505}-ceramide (Cer), into the membrane-impermeant BODIPY^{505}-SM, via the "molecular sieve" of the catalytic site of SM-synthase in the Golgi complex [61]. As shown by thin-layer fluorescent chromatography (Fig. 5A), BODIPY^{505}-Cer was efficiently converted into BODIPY^{505}-SM within 3 h. There was no detectable formation of BODIPY^{505}-GlcCer, indicating the selectivity of this SM biosynthetic pathway in CHO cells, in excellent agreement with the literature [61]. By live cell confocal imaging, incubation of CHO cells with BODIPY^{505}-Cer first produced a rather weak surface labelling (Fig. 5B,a) which could hardly be extracted using back-exchange with BSA (Fig. 5B,a′), suggesting transient retention at the PM inner leaflet, and contrasting with a major further concentration in the Golgi apparatus (Fig. 5B,c). After 1 h, micrometric patches became detected at the cell surface (not shown). After 3 h, the labelling pattern had completely shifted, due to a strong decline of Golgi labelling, concomitant with a major redistribution to brilliant cell surface patches (Fig. 5B,b,d), generating a similar signal as direct insertion of exogenous BODIPY^{505}-SM (compare peak levels of line intensity profiles in Fig. 5C with those in Fig 3B′). In contrast to the inefficacy of the initial back-exchange of BODIPY^{505}-Cer, the brilliant peripheral

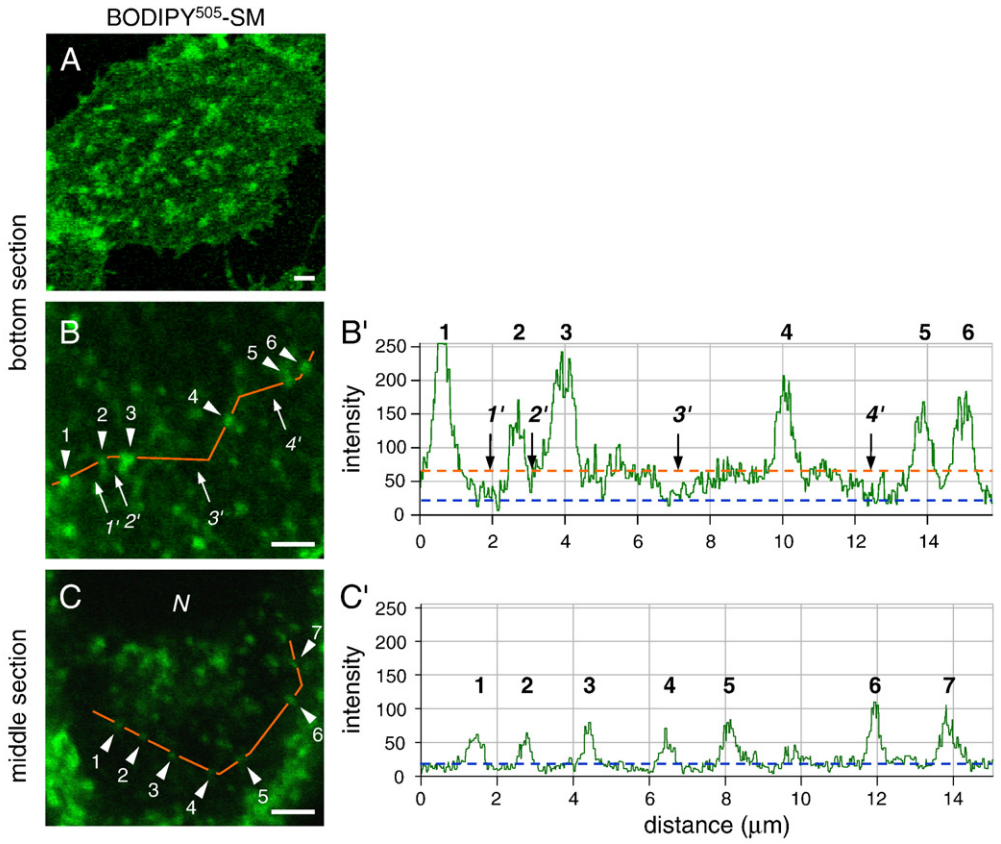

Fig. 3. In CHO cells, insertion of BODIPY^{505}-SM spontaneously labels PM (sub)micrometric patches, as in erythrocytes. At left, CHO cells were surface-labelled at 4 °C with BODIPY^{505}-SM, washed and briefly transferred to fresh medium at 37 °C before examination by confocal microscopy at the bottom cell surface (flat PM; A, enlarged at B), or in a mid-level section at the position of the nucleus (*N*; C). All scale bars, 2 µm. Right panels show line intensity profiles along the paths indicated at left by continuous orange lines. The orange broken line at B′ indicates baseline for diffuse membrane labelling above which stand labelled patches 1–6, and below which are depleted patches 1–4′, reaching fluorescence background (blue broken line). At C′, notice the lower intensity of the 7 indicated peripheral endosomes.

micrometric patches observed after 3 h entirely disappeared upon back-exchange at 4 °C (Fig. 5B,b′), demonstrating secondary incorporation into the PM outer leaflet. We concluded that the "one molecule at a time" conversion of BODIPY^{505}-Cer into BODIPY^{505}-SM by the selectivity of the catalytic site of SM-synthase, followed by inclusion into constitutive secretory vesicles and fusion with the PM, ruled out the possibility that BODIPY-SM fluorescent patches on CHO cells reflected insertion of aggregates into the PM outer leaflet.

3.7. Evidence that BODIPY-SM micrometric patches reflected endogenous SM domains and resulted from clustering into ordered domains

To further address the possibility that, once BODIPY^{505}-SM was inserted at the PM as individual molecules, substitution by the fluorophore of its alkyl chain would cause secondary aggregation, three additional controls were carried out. In a first approach, we looked at the molecular organization of BODIPY^{505}-SM patches, for which we exploited the concentration-dependent spectral properties of BODIPY^{505}-lipids. As recently reported for BODIPY^{505}-D-*e*-lactosylceramide (BODIPY^{505}-D-*e*-LacCer) at 5 µM, this family of fluorescent probes may form excimers when in very close proximity due to clustering in ordered domains, resulting in a partial shift of the primary emission peak at 520 nm ("green") to a secondary emission peak at 605 nm ("red"), generating a combined yellow signal [34]. We therefore inserted BODIPY^{505}-PC, -D-*e*-LacCer or -SM at 5 µM into CHO cells and looked for both green and red fluorescence emission. We readily confirmed the generation of yellow fluorescence with BODIPY^{505}-D-*e*-LacCer in these cells (data not shown) and extended this observation to BODIPY^{505}-SM at 37 °C at the bottom (Fig. 6A–C) and lateral PM (Fig. 6A′–C′), but not to BODIPY^{505}-PC (data not shown). Thus, BODIPY^{505}-SM clustered in ordered domains.

In a second approach, we further looked for the possibility that endogenous (unlabelled) SM would also self-associate and form domains together with its BODIPY analog, by testing whether endogenous SM depletion would impair BODIPY^{505}-SM micrometric domain formation. To this aim, a reversible, selective ~50% SM depletion was first achieved by acute sphingomyelinase (SMase) treatment (Supplementary Table 2). Alternatively, since SMase produces several side-effects, such as induction of a special type of macropinocytosis [62] or generation of ceramide, a signalling molecule that can trigger apoptosis [63], cells were treated with the dihydroceramide synthase inhibitor, fumonisin B1 (FB1), which depleted both SM and GSLs, but did not lead to ceramide accumulation. Remarkably, both SMase and FB1 strongly decreased the size of BODIPY^{505}-SM fluorescent domains (Fig. 6E,F), indicating that endogenous SM was required for micrometric BODIPY^{505}-SM PM domain formation and/or maintenance. These two lines of investigation supported the validity of BODIPY^{505}-SM as a qualitative surrogate tracer of endogenous SM, at least for the purpose of our experiments.

Incidentally, an alternative approach was used to look for the spontaneous formation of micrometric lipid domains at the outer PM leaflet, based on transfection with a GPI-GFP expression vector, which avoids issues related to intramembrane lipid tail substitution. As shown by Fig. 6G,G′,H, GPI-GFP micrometric patches were also readily detected. Thus, a totally different approach revealed similar membrane domains in CHO cells as chain-labelled fluorescent lipid probes. However, GPI-GFP micrometric patches did not codistribute with BODIPY-SM, but associated instead with BODIPY-D-*e*-LacCer at 37°C (data not shown),

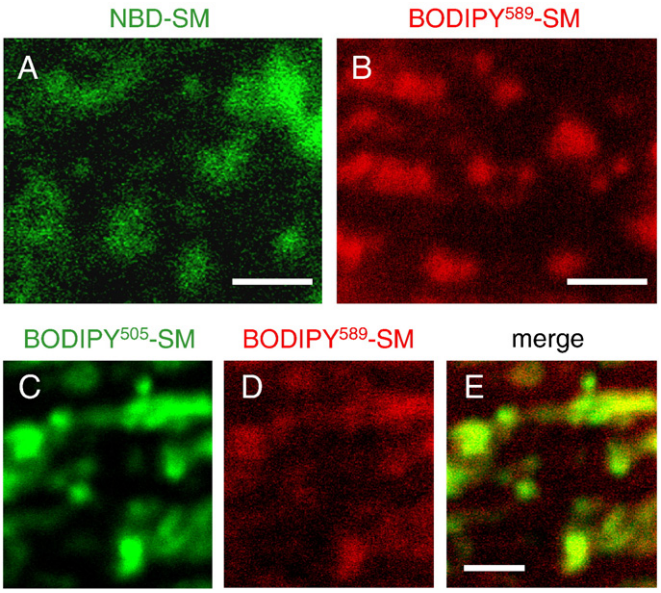

Fig. 4. Patchy BODIPY^{505}-SM PM labelling is not due to this specific fluorophore: in CHO cells, similar (sub)micrometric patches are labelled by three SM analogs bearing unrelated fluorophores. Upper panel: CHO cells were surface-labelled with NBD-SM (A) or BODIPY^{589}-SM (B), washed and transferred to fresh medium at 37 °C for immediate recording in the green and the red channels, respectively. Lower panel: CHO cells were simultaneously labelled at 4 °C with BODIPY^{505}- and BODIPY^{589}-SM at 4 °C, washed, transferred to fresh medium at 37 °C and sequentially examined in the green (C) and red channels (D). Despite lower intensity and resolution for BODIPY^{589}-SM (red), the merged image at (E) shows perfect co-localization, irrespective of structural differences of the fluorophores (shown at Supplementary Fig. 1). All scale bars, 2 μm.

further pointing to the coexistence of biochemically distinct micrometric domains at the cell surface (for a more direct demonstration, see below Fig. 8; and D'auria et al., manuscript in preparation).

3.8. BODIPY-SM micrometric domains on CHO cells did not reflect anatomical surface features nor directly associated with cortical actin patches

In contrast to the smooth-membraned erythrocytes, CHO cells bear peripheral actin-based structures, either as membrane extensions such as filopodia, microvilli and ruffles, or intracellular stress fibers and focal adhesion plaques. Since large patches of dehydroergosterol and of phosphatidylinositol 4,5-bisphosphate (PIP_2) at the inner PM leaflet were reported to merely reflect increased lipid content in proportion to increased membrane surface in folds and ruffles rather than lipid enrichment in flat micrometric domains [38,39], and since BODIPY-SM patches appeared frequently aligned in CHO cells, it was necessary to test for their relation with the actin cytocortex. To this aim, two types of experiments were carried out. First, the topology of BODIPY^{589}-SM micrometric patches was examined in YFP-actin-expressing cells. As expected, YFP-actin decorated cell bottom stress fibers and co-linear submicrometric patches (Fig. 7A,C,D), presumably focal adhesions (arrows in Fig. 7D), but these were totally segregated from BODIPY^{589}-SM domains (Fig. 7B; better seen in the merge in Fig. 7C). Second, whereas YFP-linked cortical microfilaments completely vanished upon latrunculin B treatment (Fig. 7E), BODIPY-SM patches were totally insensitive to this treatment (Fig. 7G). In addition to distinct labelling intensities (Supplementary Fig. 2), these experiments thus ruled out that BODIPY-SM micrometric patches were simply actin-dependent surface extensions, and further indicated that they reflected actin-independent, intrinsic PM domains.

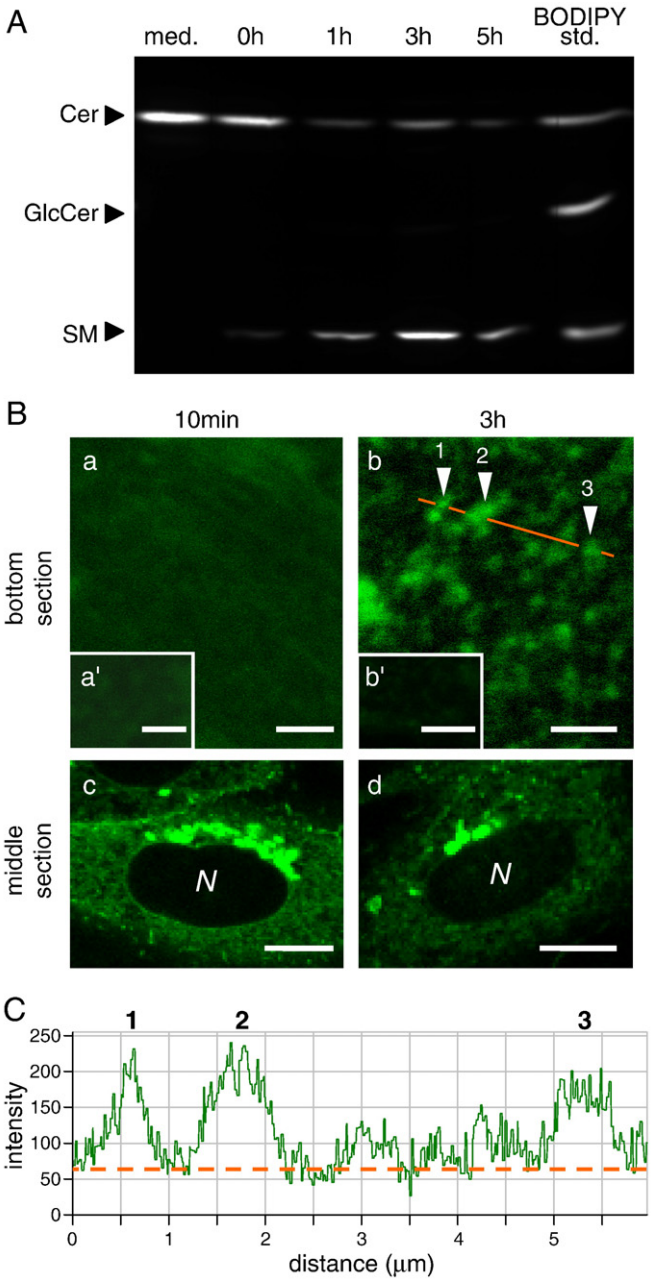

Fig. 5. BODIPY^{505}-SM patches do not reflect insertion aggregates: metabolic generation of BODIPY^{505}-SM upon BODIPY^{505}-ceramide processing produces similar micrometric PM patches as its direct insertion. CHO cells were surface-labelled with BODIPY^{505}-ceramide and incubated at 37 °C for the indicated times. (A) Kinetics of BODIPY^{505}-ceramide processing into BODIPY^{505}-SM. Medium (med.) and cell extracts collected at the indicated times of incubation at 37 °C were analyzed by TLC. Standards of BODIPY^{505}-ceramide (Cer), -glucosylceramide (GlcCer) and -SM were resolved in the right lane. Notice the exclusive conversion of BODIPY^{505}-Cer by CHO cells into BODIPY^{505}-SM, with maximal efficiency after 3 h. (B) Subcellular translocation of BODIPY^{505}-tracer. Bottom sections (scale bars, 2 μm) and mid-level confocal sections (scale bars, 10 μm) were recorded after 10 min (a,c) or 3 h (b,d). Parallel cells were submitted to surface back-exchange prior to examination (a′,b′). A low but significant fluorescence is detected at a,a′ (compare with negligible background at [c,d] in the nuclear optical section (*N*) and outside cells). The comparable labelling intensity before and after surface back-exchange (a *vs* a′) is consistent with rapid flip-flop to the inner PM leaflet, followed by rapid concentration in the Golgi complex (c). After 3 h, the probe has translocated back to the PM (b), where it is then fully removable by back-exchange (b′, compare with [a′]). (C) Intensity profile. The three numbered micrometric surface patches identified along the orange line at (B,b) exhibit a strong enrichment over the diffuse PM labelling (baseline).

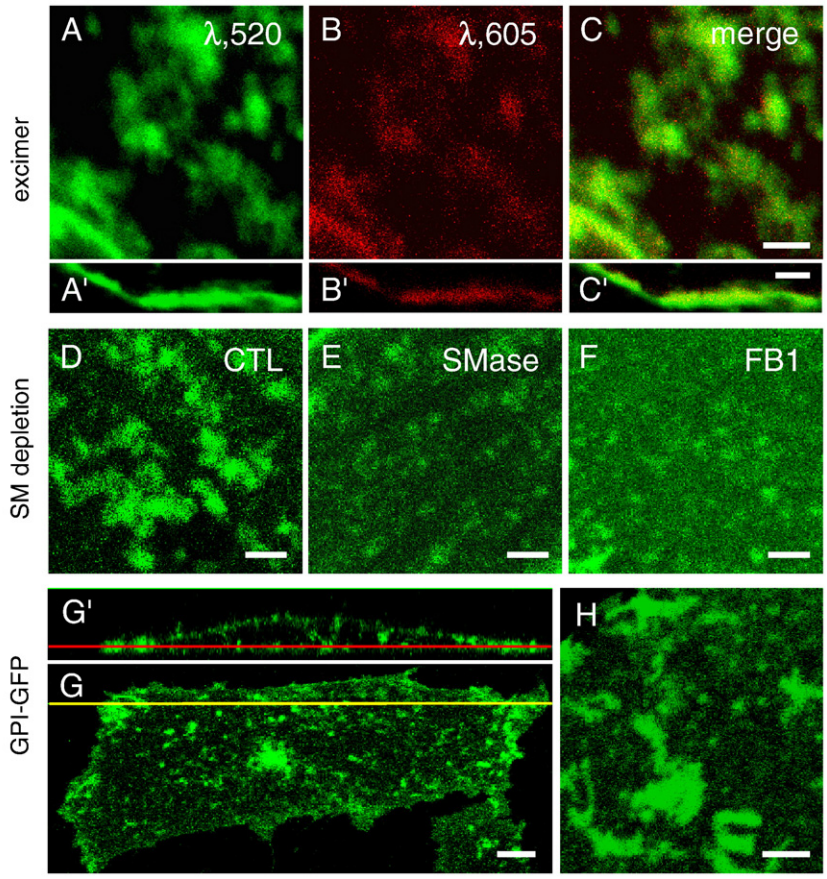

Fig. 6. Micrometric BODIPY^{505}-SM patches at the PM of CHO cells reflect clustering into ordered domains and depend on endogenous SM. (A–C) BODIPY^{505}-SM patches produce excimers. CHO cells were surface-labelled with a 5-time higher concentration of BODIPY^{505}-SM than above (5 μM), washed, transferred to fresh medium at 37 °C and immediately examined by confocal microscopy at the same temperature, using excitation at λ 488 nm. Images of the bottom PM viewed "en face" (A–C) or of the lateral PM of another cell (A′–C′) were simultaneously recorded in the green channel (A,A′; λ 520) and red channel (B,B′; λ 605), then merged (C,C′): yellow domains in merged images reveal ordered clustering. (D–F) BODIPY^{505}-SM patches depend on endogenous SM. CHO cells were left untreated (D, CTL), rapidly depleted of endogenous SM using 0.5 h-sphingomyelinase exposure (E, SMase) or depleted in sphingolipids by a 2-days inhibition with fumonisin B1 (F, FB1), then surface-labelled with BODIPY^{505}-SM, washed and directly examined by confocal microscopy. Either treatments led to ~40% SM depletion (see Supplementary Table 2) and caused almost vanishing of BODIPY^{505}-SM domains. (G–H) GPI-anchored-GFP also forms (sub)micrometric patches. CHO cells were transfected with an expression vector for glycosylphosphatidylinositol-anchored GFP (GPI-GFP) and examined after 24 h. Panel (G) shows a bottom section along the red line indicated at the vertical section above (G′). A higher magnification from another cell is shown at (H). All scale bars, 2 μm, except 5 μm at (G,G′).

3.9. BODIPY-SM and -D-e-LacCer micrometric domains largely dissociated in the CHO membrane

To further rule out membrane topography as a cause of spatial variations in probe intensity over the cell surface, we performed double labelling of BODIPY^{589}-SM with another SL analog, BODIPY^{505}-D-*e*-LacCer. Because of their much lower incorporation efficiency and quantum yield, the "red" BODIPY-SM analog was inserted at higher concentrations and laser parameters in the green channel were adapted to approach a comparable signal intensity as in the red channel. Although intensity and resolution remained unequal, a major dissociation was observed between BODIPY^{589}-SM and BODIPY^{505}-D-*e*-LacCer (Fig. 8C), contrasting with the perfect co-localization between two GSL derivatives, BODIPY^{589}-GlcCer and BODIPY^{505}-D-*e*-LacCer, irrespective of their distinct head groups and different fluorophores (Fig. 8F).

3.10. Formation and maintenance of BODIPY-SM micrometric domains required energy and were controlled by cholesterol

Having collected strong evidence that BODIPY^{505}-SM domains spontaneously formed by self-clustering in ordered domains, whether using direct insertion or intracellular generation from BODIPY^{505}-ceramide, and having ruled out a variety of artefacts, we felt that it became justified to turn our attention to their biogenesis. We looked at two possible biological mechanisms whereby the size of these domains was restricted to the micrometric range in nucleated cells, beside the physical role of membrane tension already revealed in erythrocytes, namely (i) the energy-state and (ii) cholesterol dependence. To examine the role of energy, likely involved in membrane tension, cells were ATP-depleted by brief incubation with azide and deoxyglucose. As the most relevant functional assay, the efficiency of energy depletion was confirmed by a block of membrane lipid endocytosis (Fig. 9, compare A′ with C′), similar to that observed for K^+-depletion (Fig. 9B′). ATP-depletion greatly decreased the number of discrete micrometric BODIPY^{505}-SM domains, while inducing their coalescence into elongated structures (Fig. 9C). Coalescence was readily reversible, since ATP repletion rapidly caused their dispersion, back to the original pattern (Fig. 9D) and allowed BODIPY^{505}-SM endocytosis to resume (Fig. 9E′). That micrometric domains restored upon ATP repletion indeed resided at the PM was confirmed by their complete disappearance upon surface back-exchange (Fig. 9E), a procedure which fully preserved the intracellular endosomal labelling (Fig. 9E′). These complementary experiments indicated that energy was required to control the size and shape of BODIPY^{505}-SM micrometric domains at the PM, and suggested their plasticity.

Cholesterol is an essential membrane component to regulate its fluidity. Interestingly, Maxfield and coworkers have reported that

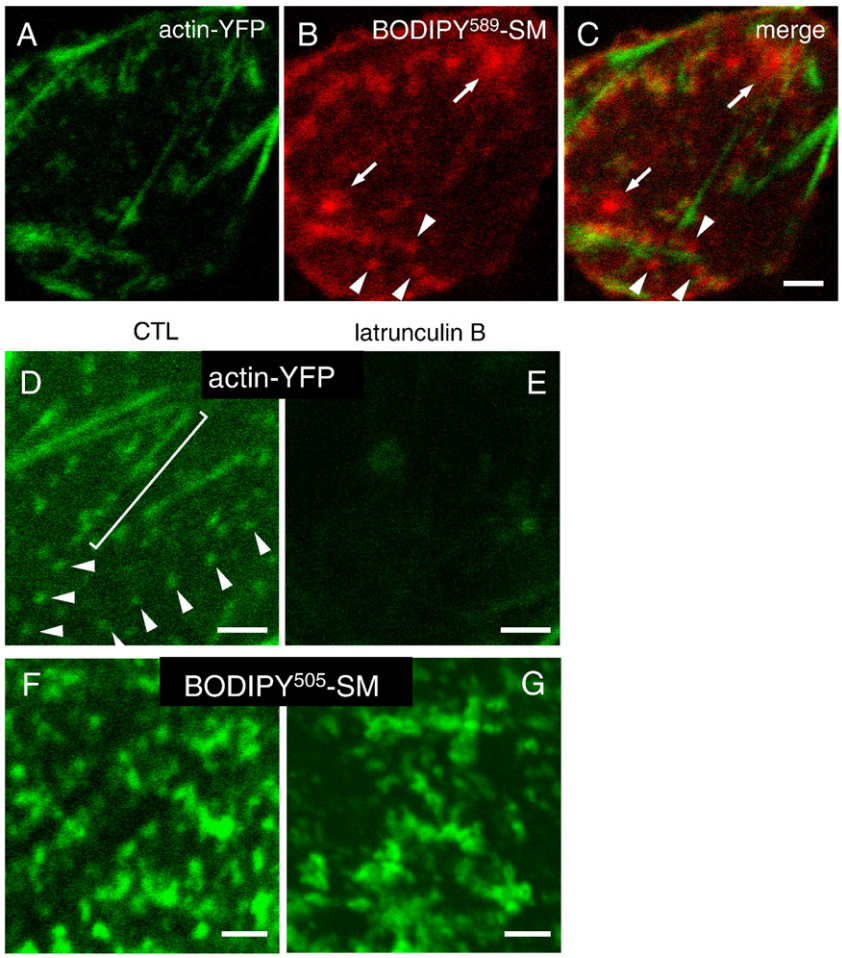

Fig. 7. Formation of BODIPY-SM (sub)micrometric domains does not require actin polymerization. (A–C) Spatial segregation: double imaging by actin-YFP and BODIPY^{589}-SM. CHO cells expressing actin-YFP (green) were surface-labelled for BODIPY^{589}-SM (red) as in Fig. 4B and the bottom cell surface was sequentially recorded in the green (A) and red channel (B), with merge at (C). Although BODIPY-SM domains are frequently aligned next to cortical actin fibers (arrowheads), they are clearly segregated therefrom. Arrows indicate alternative BODIPY-SM domains without apparent relation with microfilament-enriched domains. (D–G) Functional segregation: BODIPY-SM domains are insensitive to actin depolymerization. Actin-YFP-expressing (D,E) or not-transfected CHO cells (F,G) were either left untreated (D,F: CTL) or treated with latrunculin B (E,G). Notice at (D) peripheral fibers (elongated bracket) with co-linear focal adhesions (arrowheads at bottom); both structures disappear upon latrunculin B treatment (E). BODIPY^{505}-SM domains are undistinguishable in control (F) or latrunculin B-treated cells (G). All scale bars, 2 μm.

cholesterol depletion in CHO cells generates very large membrane domains labelled by NBD-SM [27]. In full agreement with this report, a ~70% loss of cell cholesterol by mβCD (Supplementary Table 2), which did not affect the level of BODIPY^{505}-SM insertion into the PM (data not shown), induced very large irregular surface domains (up to 5 μm^2; Fig. 9F). By contrast, overloading cell cholesterol by two-fold with mβCD:Chol complexes (Supplementary Table 2) did not appreciably affect the size, nor the abundance of BODIPY^{505}-SM surface micrometric domains (Fig. 9G). Together with reversible clustering upon ATP-depletion, these data suggested that BODIPY^{505}-SM micrometric domains were dynamic, reversible PM structures, reaching equilibrium at a size controlled by physiological concentrations of cholesterol, thus likely by membrane fluidity.

3.11. Micrometric BODIPY-SM structural compartmentation was functionally reflected by restriction of lateral diffusion in large fields

Morphological results reported thus far have revealed that BODIPY^{505}-SM spontaneously formed micrometric domains in the outer PM leaflet of erythrocytes and CHO cells, in a tension-, energy- and cholesterol-dependent manner. To pursue our analysis on the role of membrane fluidity, we next tested whether membrane boundaries of BODIPY^{505}-SM domains would influence the dynamics of its lateral diffusion, as measured by fluorescence recovery after photobleaching (FRAP). FRAP, a validated method to study the lateral mobility of defined PM constituents [35,64], is generally applied to a single constituent on a single spot area. To test for a size-restriction of BODIPY^{505}-SM domains, we were inspired by the pioneering work of Yechiel and Edidin [35], and systematically compared FRAP properties after photobleaching two different areas, of respectively 5 μm^2 (referred to as "small fields") and 20 μm^2 ("large fields"). These fields were selected to be much larger than nanometric lipid rafts, to address instead the dynamics of micrometric lipid domains, which were indeed originally inferred by FRAP using comparable field sizes [35].

Linear variations of BODIPY^{505}-SM concentration in the medium, which resulted in proportional changes of its PM content as stated above, had no influence on its FRAP parameters. As shown by Fig. 10A,B, recovery of BODIPY^{505}- and NBD-SM in large fields (20 μm^2, closed symbols) levelled off with an extrapolated mobile fraction at infinite time of recovery of 50 ± 1% (mean ± SEM; $n = 151$), but this restriction disappeared in small fields (5 μm^2, open symbols), reaching 82 ± 2% recovery (mean ± SEM; $n = 65$). The lateral diffusion properties of these two SM analogs were next compared to those of another SL analog, BODIPY^{505}-D-*e*-LacCer, which associates with a biochemically distinct

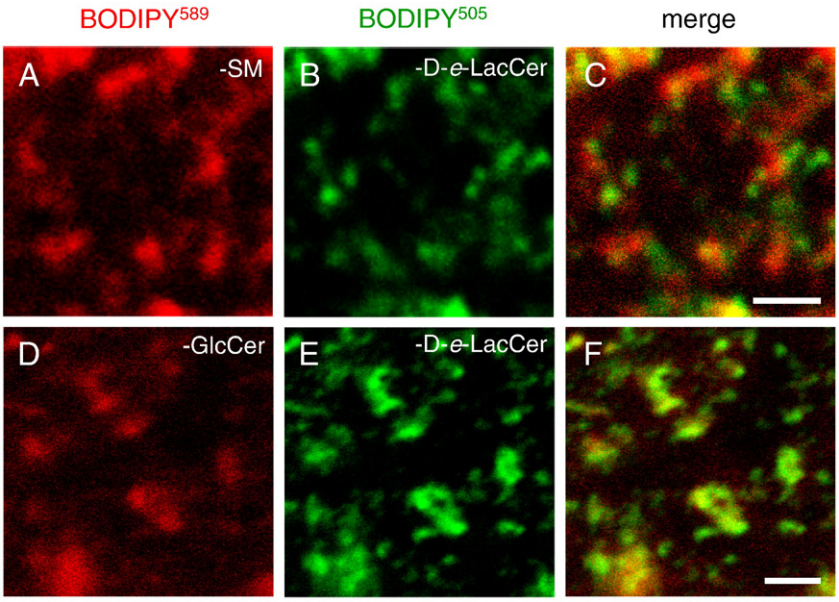

Fig. 8. Coexistence of distinct BODIPY-SM and BODIPY-D-*e*-LacCer micrometric domains in CHO cells. CHO cells were K^+-depleted to block endocytosis (see below, Fig. 9), then sequentially labelled with the indicated $BODIPY^{505}$- and $BODIPY^{589}$-lipids at 37 °C for 10 min. Images were sequentially recorded in the green (B,E) and red channels (A,D) with settings adjusted to best match signal intensities, then merged (C,F). Despite lower intensity and resolution of the red tracers, $BODIPY^{505}$- and $BODIPY^{589}$-glycosphingolipids show perfect co-localization (F). In contrast, notice extensive dissociation between $BODIPY^{505}$-D-*e*-LacCer and $BODIPY^{589}$-SM at (C). All scale bars, 2 μm.

type of PM domain (see above, Fig. 8). As shown by Fig. 10C, FRAP behaviour of $BODIPY^{505}$-D-*e*-LacCer was undistinguishable in small fields (5 μm^2) and large fields (20 μm^2), with an average mobile fraction of 65 ± 3% (mean ± SEM; $n = 54$). Thus, for both fluorescent SM analogs, about half of the surface pool encountered sustained restriction to lateral diffusion when bleached in large fields, a restriction largely relaxed when bleaching small fields; in marked contrast, the mobile fraction of the LacCer analog was similarly high, be it in small or large fields. This difference between $BODIPY^{505}$-SM and -D-*e*-LacCer was confirmed in J774 macrophages (data not shown). To the opposite, a severe restriction in both large and small fields was observed for both the self-aggregating probe, *N*-Rh-PE [65,66] (Fig. 10D), and for the Alexa 488-labelled pentameric B subunit of cholera toxin (CTXB), which binds to and clusters GM1 ganglioside (data not shown), in good agreement with previous reports [67,68].

Two additional controls were performed. Firstly, either direct PM insertion of $BODIPY^{505}$-SM or its secondary incorporation after $BODIPY^{505}$-Cer bioconversion resulted in undistinguishable mobile fractions in both large and small fields (Fig. 11A, compare left and right), further ruling out a bias by probe aggregation. Secondly, since FRAP experiments were performed at 30 °C, we considered the possibility of differential surface fluorescence loss by photobleaching (FLIP) or by endocytosis. Differential FLIP could be readily excluded, since the bleached area accounted for <2% of the cell surface and bleaching was limited to a single round of 2–3 s for $BODIPY^{505}$- and NBD-lipids. To directly rule out endocytosis, $BODIPY^{505}$-SM lateral diffusion in large fields was further studied at 37 °C after blocking endocytosis by K^+- and ATP-depletion. These procedures, which effectively blocked $BODIPY^{505}$-SM internalization (see Fig. 9), did not appreciably alter its mobile fraction (Fig. 11B). We therefore could not find methodological pitfalls that would account for the existence of micrometric domains labelled by SM analogs and for the decreased mobility of their constituents only after bleaching of large fields and thus concluded these two observations rather reflected genuine biological properties of the PM.

To finally address a possible role of cortical actin in the restriction of lateral diffusion revealed by FRAP, cells were treated with latrunculin B. In keeping with the complete resistance of $BODIPY^{505}$-SM micrometric domains to this G actin-sequestering agent, latrunculin B did not significantly affect the mobile fraction of this lipid analog after photobleaching 20-μm^2 fields (Fig. 11C).

3.12. Long-range lateral diffusion of BODIPY-SM was simultaneously favored by endogenous SM and restricted by endogenous GSLs

To finally confirm the dependence of $BODIPY^{505}$-SM domains on endogenous SM by kinetic data, cells were briefly treated by SMase as above before FRAP analysis. The ~50% total SM depletion decreased the $BODIPY^{505}$-SM mobile fraction in large fields by two-fold (Fig. 11D, hatched bar), which was restored by natural SM repletion from serum (Fig. 11D, grey bar). To verify that SMase effects on $BODIPY^{505}$-SM diffusion were due to SM depletion, and not to ceramide accumulation, cells were treated with fumonisin B1 (FB1), which leads to a combined inhibition of SM and GSLs biosynthesis without causing ceramide accumulation, then surface-labelled with $BODIPY^{505}$-SM without or after selective replenishment with two short-chain non-fluorescent analogs, C_6-SM or C_8-ceramide [42,69]. These readily incorporatable SLs, albeit with shorter alkyl chains, conserve interfacial regions and head groups, thus preserve some competence for lipid:lipid interactions [for a review, see 52]. As shown by Fig. 11E, whereas combined SLs depletion by FB1, without or after replenishment by C_8-Cer, had no significant effect on $BODIPY^{505}$-SM lateral diffusion (two hatched bars), replenishment with C_6-SM selectively increased its mobile fraction in large fields, to a level close to that observed in small fields (grey bar). These experiments ruled out that SMase effects were due to ceramide accumulation and indicated instead that long-range mobility of $BODIPY^{505}$-SM selectively depended on SM.

Surprisingly, these experiments also pointed to an opposite effect of endogenous SM and GSLs on $BODIPY^{505}$-SM lateral diffusion. Indeed, combined SM and GSLs depletion had no significant effect, while reloading with C_6-SM alone appeared sufficient to relax the restriction to its lateral diffusion in large fields. To further test for such an opposite effect of SM and GSLs, FB1-treated CHO cells were alternatively replenished with the non-fluorescent GSL, GM3. As predicted, GM3

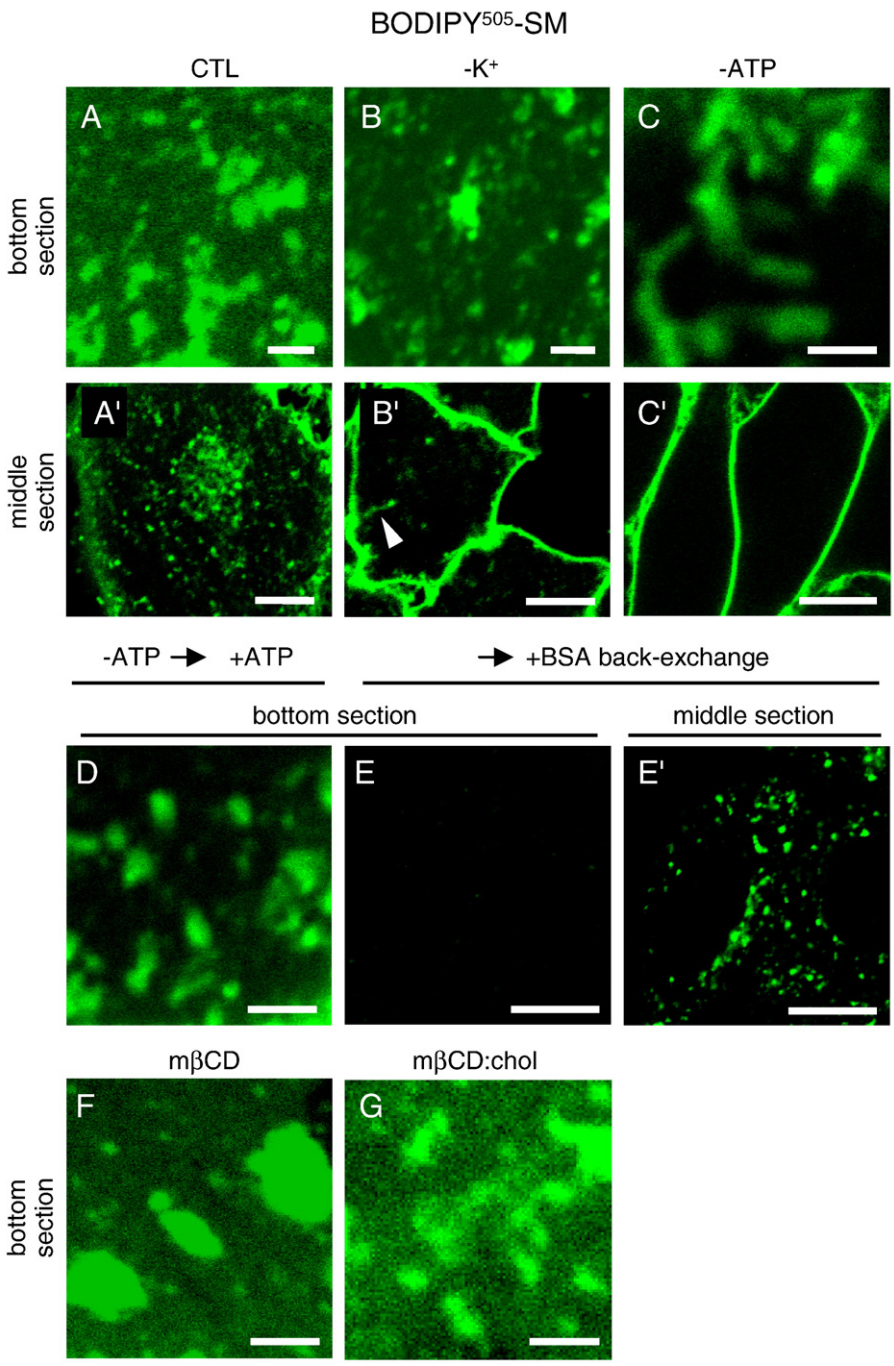

Fig. 9. BODIPY-SM micrometric domains depend on energy and cholesterol, but not on endocytosis. CHO cells were kept untreated (A,A′; CTL); K^+-depleted (B,B′; $-K^+$); energy-depleted (C,C′; − ATP), then repleted (D,E,E′; →+ATP) and some of them were further submitted to a surface back-exchange procedure (E,E′). In parallel, cells were either extracted with empty methyl-beta-cyclodextrin (F, mβCD; ~70% cholesterol depletion), or incubated with mβCD:Chol (G, ~2-fold free cholesterol overload). Thereafter, cells were surface-labelled with BODIPY^{505}-SM as usual, washed and the bottom PM (A–C, D–G, scale bars, 2 μm) or mid-level confocal sections (A′–C′, E′; scale bars, 10 μm) were recorded at ~20 min after transfer to 37 °C. In control conditions, the BODIPY^{505}-SM labelling pattern is clearly distinct between the cell surface (A) and endocytic vesicles (A′). Panels (C′,B′) illustrate the efficiency of the endocytic block after ATP- or K^+-depletion (the very limited "intracellular" labelling at B′ may be continuous with the cell surface, see arrowhead). Notice the persistence of micrometric BODIPY^{505}-SM PM domains despite endocytic block (B,C). Panels (E,E′) demonstrate the reversibility of the endocytic block upon ATP repletion. Finally, notice that BODIPY^{505}-SM domains coalesce upon cholesterol depletion (F), but do not shrink upon cholesterol overload (G).

replenishment further decreased BODIPY^{505}-SM mobile fraction in large fields (Fig. 11E, dotted bar). Altogether, these results confirmed that endogenous GSLs and SM exerted opposite effects on BODIPY^{505}-SM long-range lateral diffusion, which was favored by endogenous SM and concomitantly restricted by endogenous GSLs. The implications of these observations for the simultaneous existence of distinct PM lipid domains and their mechanistic explanation require further investigations.

4. Discussion

4.1. Overview

We here report that fluorescent SM analogs spontaneously cluster into micrometric domains with lipid phase behaviour at the outer PM leaflet of erythrocytes and CHO cells under physiological conditions. This conclusion is supported by: (i) confocal imaging

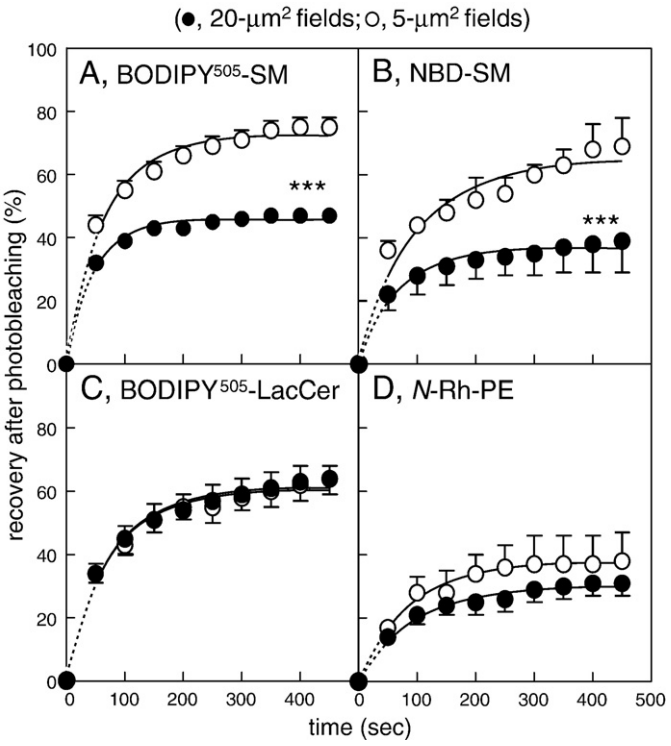

Fig. 10. Selective restriction of SM lateral diffusion in large fields. CHO cells were surface-labelled with BODIPY^{505}-SM (A), NBD-SM (B), BODIPY^{505}-D-*e*-LacCer (C) or the self-clustering probe, *N*-Rh-PE (D), rapidly washed and immediately analyzed by FRAP at 30 °C with a Bio-Rad MRC1024/Axiovert M135 or a Zeiss LSM510 confocal microscope in fields of either 20 μm^2 (filled symbols) or 5 μm^2 (open symbols). Fluorescence recovery is expressed as percentage of signal before photobleaching, after correction for residual fluorescence immediately after bleaching. Values are means ± SEM of 3-to-112 experiments and are fitted to monoexponential functions. Notice the restricted diffusion of the two SM analogs when analyzed in large fields (A,B), contrasting with the same lateral diffusion in large and small fields for BODIPY-D-*e*-LacCer (C) and the very low diffusion of the self-clustering probe *N*-Rh-PE (D), irrespective of field size. Discontinuous lines indicate low accuracy of early values with the Bio-Rad equipment. ***, $p<0.001$.

with three different analogs combined with variations of temperature, membrane tension and cholesterol content; (ii) kinetic analyses by FRAP in two different field sizes; and (iii) exclusion of multiple artefacts including fluorescent lipid aggregates, surface structural features such as actin-dependent projections or "echinocyte" transformation due to insertion of amphiphilic probes, as well as endocytic structures. We finally propose three, non-mutually exclusive, mechanistic interpretations. Firstly, fluorescent SM micrometric patches reflect clustering in ordered domains, as suggested by BODIPY excimer formation. Secondly, these fluorescent domains are defined in (i) shape by liquid-phase coexistence, directly visualized by double labelling of BODIPY-SM and -LacCer, and (ii) size by membrane tension and intrinsic fluidity, as suggested by reversible hypotonicity and cholesterol depletion. Thirdly, fluorescent SM domains presumably reflect preexisting domains spontaneously enriched in endogenous SM, based on reversible SM depletion by sphingomyelinase and selective replenishment by C_6-SM after pharmacological inhibition of upstream biosynthetic pathways. The latter interpretation admittedly remains speculative, and calls for considerable further investigations.

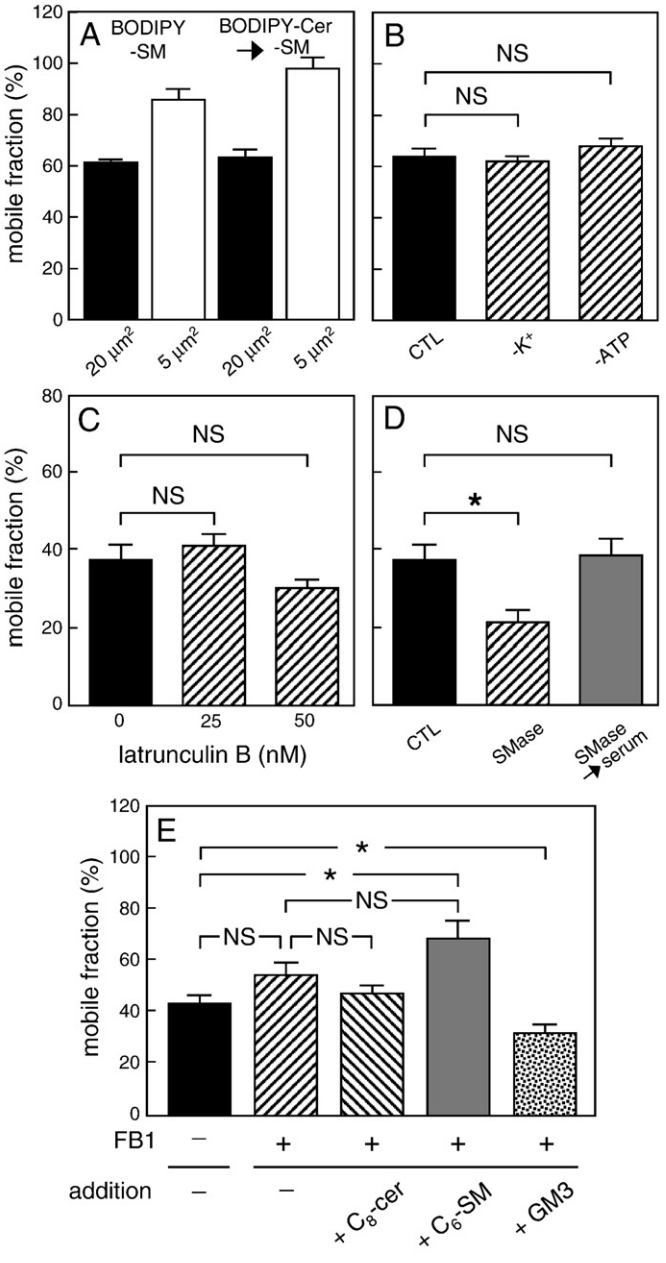

Fig. 11. Restriction to lateral diffusion of BODIPY^{505}-SM in large fields does not reflect self-aggregation (A), endocytosis (B), nor cortical actin (C), but depends on endogenous SM and GSLs (D,E). (A) Similar mobile fraction of BODIPY-SM after direct insertion or conversion from its ceramide precursor. CHO cells were surface-labelled by exogenous BODIPY-SM as usual or by endogenous BODIPY-SM converted from its ceramide precursor after 3 h as in Fig. 5B,b, then analyzed by FRAP at 30 °C in fields of either 20 μm^2 (filled bars) or 5 μm^2 (open bars), as in Fig. 10. Mobile fraction values at infinite time of recovery were derived by monoexponential fitting and are means ± SEM of 4 to 60 experiments. (B) Large-field restriction of BODIPY-SM does not depend on endocytosis. Control (CTL), K^+-depleted ($-K^+$), or energy-depleted CHO cells ($-$ATP) were surface-labelled with BODIPY-SM, rapidly washed and immediately analyzed in corresponding media by FRAP using 20-μm^2 fields. Mobile fractions are means ± SEM of 5-to-14 experiments. (C) Large-field restriction of BODIPY-SM does not depend on actin microfilaments. CHO cells were either kept untreated (filled bar) or treated at 37 °C for 30 min with 25 or 50 nM latrunculin B (striped bars), then surface-labelled with BODIPY-SM, washed and analyzed by FRAP in the same medium in 20-μm^2 fields. Values are means ± SEM of 3-to-6 experiments. (D) Large-field diffusion of BODIPY-SM requires endogenous SM. CHO cells were kept untreated (filled bar), rapidly depleted of endogenous SM (SMase, hatched bar), or further allowed to recover SM from serum (grey bar), then surface-labelled with BODIPY-SM, washed and analyzed by FRAP in 20-μm^2 fields. Mobile fractions are means ± SEM of 3-to-16 experiments. (E) Selective replenishment of SL-depleted cells by short-chain SM or GM3 have opposite effects on BODIPY-SM diffusion in large fields. CHO cells were kept untreated (filled bar) or treated for 2 days with fumonisin B1 (FB1; hatched bar). Treated cells were left depleted or selectively replenished with C_8-Cer, C_6-SM or GM3 at 4 °C as indicated, then surface-labelled with BODIPY-SM, washed and analyzed by FRAP in 20-μm^2 fields. Mobile fractions are means ± SEM of 5-to-12 experiments. N.S., not significant; *, $p<0.05$.

4.2. Why is the existence of micrometric PM domains in living cells controversial?

SM, a major constituent of the outer PM leaflet, is now well-accepted to cluster with cholesterol in dynamic nanometric lipid rafts [4,5,18,19], but these fall below the detection limit of conventional fluorescence microscopy [for reviews, see 12,21]. In contrast, we readily observed micrometric PM patches by confocal microscopy imaging in all living cells tested. Since insertion aggregates, structural and imaging artefacts could be reasonably excluded, why is the existence of micrometric PM domains a matter of dispute [for a recent review, see 21]?

The concept of discrete micrometric PM lipid domains inserted into a continuous distinct phase at the surface of living nucleated cells was proposed two decades ago by Yechiel and Edidin as a first refinement of the original fluid mosaic model, by inference from FRAP evidence that lateral diffusion of NBD-PC was restricted in large but not in small fields [35]. Unfortunately, although images of NBD-PC-labelled cell surface were simultaneously provided, they remain difficult to interpret since only very large (>10 μm), single spots were reported. Moreover, the validity of the concept of micrometric domains became questioned after several other groups did not find evidence for such restriction, although their study was limited to small or undefined bleached field sizes [64,70]. Several groups further attempted to visualize micrometric domains by exploiting the major technical developments of confocal microscopy, but could not reach conclusions applicable to living and untreated cells, raising instead major doubt on their very existence. Two types of objections were raised. First, morphological evidence of large lipid domains was mainly based on insertion of fluorescent analogs into non-living systems, such as liposomes or GPMVs [22–24]. Second, formation of fluorescent membrane lipid domains visible by confocal microscopy in living cells required major alterations in their lipid contents. For instance, it was reported that surface digestion of erythrocyte membranes by phospholipase C/sphingomyelinase led to the formation of micrometric domains enriched with fluorescent ceramide [26]. Likewise, lowering cholesterol levels induced the formation of visible micrometric domains on several mammalian cell types [27]. It is, however, no surprise that these very artificial conditions led instead to the opposite suggestion, i.e. that the formation of such micrometric membrane domains in untreated living cells is actually prevented, due to interactions with membrane proteins and with the cytoskeleton [24].

However, phase coexistence of micrometric membranes could be documented in living cells, in rare cases with unquestionable approaches, but more often under non-physiological temperature, which left critical readers sceptical on the whole concept. In living erythrocytes, phase coexistence has been evidenced by: (i) Laurdan general polarization (GP) values at 25–35 °C, which detected lipid order and phases [28]; (ii) phase mapping, which distinguished two types of domains showing either low fluidity, low spacing and high order; or higher fluidity and larger spacing [29]; and (iii) FTIR (Fourier transform infrared spectroscopy), which unravelled multiple sharp membrane phase transitions at 4 °C [30]. On living blood platelets, the distribution of the L_o-lipidomimetic synthetic dye DiIC18 was reported to be inhomogeneous around 24 °C [31,32]. In nucleated cells, micrometric membrane patches with phase separation have been clearly reported: (i) in CHO cells with NBD-SM, but not DiIC16, at 33–34 °C [27]; (ii) in macrophages with Laurdan GP values at physiological temperatures [33]; and (iii) in fibroblasts with BODIPY-L-*t*-LacCer at 10 °C [34].

Our studies identify four reasons that could explain why micrometric lipid membrane domains may so far have been missed or neglected: (i) membrane composition; (ii) temperature of examination; as well as (iii) nature and (iv) spectral properties of tracers. The first parameter is membrane composition, in particular a low-to-moderate cholesterol content. Thus, in cholesterol-poor human platelets (~15% molar concentration) or in giant unilamellar vesicles (GUVs) mimicking their lipidic composition, DiIC18 micrometric domains readily formed at 24 °C, but not after doubling the cholesterol content [31,32]. These DiIC18-enriched domains were irregular in shape, which is generally considered to reflect the coexistence of L_d/solid-ordered (S_o) phases [32]. Cholesterol is concentrated at the boundaries of these coexisting phases where it reduces line tension [for a review, 14]. Since, in contrast to the cholesterol-poor platelet membrane, the erythrocyte PM contains >40 mol% of cholesterol [32,71], L_d/S_o phases are not expected to coexist in these cells so that DiIC18 would not form micrometric domains, as observed by other investigators [26,30] and confirmed in our study. In contrast to the irregular DiC18 domains observed on blood platelets, we found that BODIPY-SM and -GlcCer domains on erythrocytes were perfectly round. A regular shape implies that these domains reflect instead liquid-phase coexistence [20], which could be evidenced in erythrocytes despite their high cholesterol content. Indeed, the role of cholesterol in the liquid-phase separation is to increase the lipid membrane ordering throughout the L_o-phase, to such an extent that the system finally favors a separation between L_o- and L_d-phases [72]. Besides cholesterol, we found that the abundance of sphingolipids (see Fig. 6E,F and Fig. 11E) is another key player for micrometric domain formation and motility [see also 21,36].

A second critical parameter for micrometric lipid domain visualization is the temperature of examination. Indeed, the number of BODIPY-SM circular domains we observed at the free hemi-erythrocyte surface strongly depended on temperature, with a peak at 20 °C and a substantial decrease above, the distinct behaviour of BODIPY^{505}-GlcCer with steady increase up to 37 °C serving here as an informative internal control. This result on living cells is consistent with previous observations on GUVs, in which cholesterol and SM form microscopically observable circular L_o-phase domains only below the Tm of the SM species used [for a review, 52]. Likewise, at the erythrocyte membrane, Laurdan GP values peak at 25–30 °C and decrease at higher temperatures [28]. In polarized epithelial cells, the apical membrane also exhibits a temperature-dependent phase behaviour. This unique "macroscopic" membrane domain is equivalent to a continuous raft phase below 25 °C, whereas at 37 °C rafts individualize within a non-raft phase [36].

A third limiting factor for the visualization of micrometric lipid domains is probably related to the structural properties of the tracers used as fluorescent analogs, namely the very nature of the polar headgroups and their alkyl tail lengths. The nature of the polar headgroup is most likely the major factor here at play. Indeed, changing the BODIPY^{505}-sphingolipid headgroup from phosphocholine (in BODIPY^{505}-SM) to glucose (in BODIPY^{505}-GlcCer) respectively led to maximal domain formation at 20 °C and at 37 °C. These differences must be related to lipid partitioning, since the bulk membrane tracer, TMA-DPH, produced uniform erythrocyte labelling whatever the temperature. Moreover, as shown by BODIPY^{505}-ceramide, the very presence of a polar headgroup may be essential for stable association with the outer leaflet and domain formation therein. Indeed, whereas we found that BODIPY^{505}-SM remained fully associated with the outer PM leaflet at 4 °C (since fully extractable by BSA back-exchange), BODIPY^{505}-ceramide spontaneously translocates into the inner PM leaflet (as shown by resistance to surface back-exchange), before slow shuttling to the Golgi complex and processing into BODIPY^{505}-SM. Incidentally, whether membrane lipids can form stable domains organization at the inner leaflet is essentially unknown. In this respect, the cell surface pool of BODIPY^{505}-ceramide that was resistant to surface back-exchange (i.e. *bona fide* translocated to the inner leaflet, and remaining for an extended period therein) did not form any detectable domain. With respect to the alkyl tail length, our preliminary recent observations indicated that incubation of erythrocytes with BODIPY^{505}-SM conjugates where the fluorophore is

grafted at C_{12} of the fatty acid alkyl tail (instead of C_5 as generally used in our study) produced at 20 °C a diffuse labelling detectable upon higher laser power, without micrometric patches (data not shown), in agreement with a previous report [26]. These observations could be explained if the longer the side-chain, the higher the Tm, so that domains would only form at higher temperature. However, this interpretation calls for further analyses, combined with a systematic screen of variations in membrane tension and cholesterol depletion/overload, in order to feed biophysical modelling.

Fourthly, the unique spectral properties of BODIPY^{505} in comparison to the more commonly used NBD could also explain why micrometric domains may have been frequently overlooked in the past. As compared with BODIPY^{505}, the other fluorophores that we used required much higher laser power, due to lower insertion efficiency (BODIPY^{589}) and/or lower quantum yield (NBD), thus inevitably causing accelerated photobleaching, if not being intrinsically more sensitive to photodamage (NBD). While we could undoubtfully detect micrometric fluorescent patches at 37 °C using SM coupled to NBD and BODIPY^{589} under optimal observation conditions, we would probably have missed these observations, should we not have started our investigations with BODIPY^{505}-SM.

4.3. Micrometric fluorescent SM patches are genuine PM features, not aggregation or light-induced artefacts, nor peripheral endosomes

Several lines of evidence allow us to exclude aggregation and artificial partitioning artefacts. Firstly, this report was primarily based on the visualization at physiological temperature of fluorescent micrometric PM domains on erythrocytes and nucleated cells, after either (i) direct insertion of three fluorescent SM analogs presented as complexes with BSA, prepared by a conventional or by a more elaborated procedure involving extensive dialysis and ultracentrifugation, or (ii) intracellular bioconversion of BODIPY-ceramide into BODIPY-SM followed by vesicular transfer to the PM. When completed, both procedures led to tracer levels of incorporation as compared with endogenous SM and allowed full removal using surface back-exchange with BSA. In view of two-step filtering of the bioconversion/exocytosis approach, respectively by the catalytic site of SM-synthase and by the quality control machinery for Golgi vesicular exit, we consider that BODIPY-Cer bioconversion experiments provide compelling evidence against aggregation artefacts. Secondly, the vast majority of cell surface BODIPY-SM showed rapid lateral diffusion in small fields, whereas the self-aggregating *N*-rhodaminylphosphatidylethanolamine [66] or CTXB-cross-linked GM1 essentially occurred as immobile patches, indicating that aggregation of the fluorescent membrane probes we used could have been readily evidenced. Moreover, aggregation could hardly explain consistent differences in FRAP between 20- and 5-μm^2 fields for SM analogs, contrasting with the similar recovery in both field sizes for the GSL analog, BODIPY^{505}-D-*e*-LacCer. We conclude that micrometric BODIPY-SM patches do not reflect aggregation or artificial partitioning artefacts.

It has been reported that continuous illumination of GUVs bearing a fluorescent dye eventually (after ~15 s) induces artificial partitioning artefacts into highly non-random bilayer mixtures [73]. Factors involved in this artefact include composition, mode of preparation and dye concentration, but neither the type of dye (whatever BODIPY, DiI, Texas red etc… were used), nor the temperature (since phase separation progressed after ~15 s at the same kinetics at 10 °C and 23 °C). However, micrometric domains we observed in erythrocytes cannot be explained by this artefact since: (i) they were observed at the very first scan and did not increase with time; (ii) their formation showed a very distinct response to temperature between BODIPY-SM and -GlcCer, both used at 1 μM; (iii) no phase separation was obtained with BODIPY-GlcCer at 10 °C or 20 °C and with DiIC18 and TMA-DPH, whatever the temperature.

A role for endocytosis in micrometric SM domains biogenesis can also be excluded. Firstly, micrometric BODIPY-SM domains were readily observed on erythrocytes, which are totally endocytosis-defective. Secondly, under appropriate conditions, micrometric BODIPY-SM domains visualized on nucleated cells completely disappeared after surface back-exchange, demonstrating exclusive cell surface residency (data not shown). In particular, micrometric organization viewed by confocal microscopy and supported by long-range lateral diffusion properties by FRAP both resisted endocytosis block by K^+- and ATP-depletion. Thirdly, surface back-exchangeable BODIPY^{505}-SM domains completely differed from endosome-associated tracer by size, intensity and localization. Fourthly, we had noticed that it took <5 min to reach maximal FRAP recovery of BODIPY^{505}-SM, both in large fields (mobile fraction of ~50%) and small fields (~80%). We further verified that, after this brief interval at 37 °C, <12% of the total label initially incorporated at 4 °C had acquired resistance to subsequent back-exchange at 4 °C (data not shown). We conclude that micrometric domains formation did not require endocytosis, which also did not significantly contribute to large-scale restriction of BODIPY^{505}-SM lateral diffusion, as measured by FRAP.

4.4. Micrometric BODIPY-SM patches do not reflect structural PM features, thus qualify as PM lipid domains

Due to the limited resolution of confocal fluorescence microscopy, exclusion of surface topology features (e.g. [clustering of] membrane projections with uniform labelling intensity per unit surface) was essential before considering the existence of "domains with focal lipid enrichment". We will first discuss the role of actin-based surface projections, then the artificial induction of membrane spicules due to unequal partition of amphiphiles between the two membrane leaflets. Firstly, scanning electron microscopy demonstrated that the erythrocyte surface was totally devoid of (sub)micrometric surface features, both in the relaxed and stretched states, and so remained after BODIPY-SM insertion. Secondly, membrane insertion of two totally unrelated lipidomimetic dyes: DiIC18, which was reported to diffusely label the erythrocyte membrane at 4 °C and 20 °C [26,30], and TMA-DPH, a well-accepted bulk membrane tracer [53,54], showed no micrometric labelling whatever the temperature tested, strongly arguing against local clusters of membrane projections. Thirdly, BODIPY-SM patches on erythrocytes were insensitive to latrunculin and did not disappear (instead coalesced) upon stretching by hypotonic swelling. We thus conclude that (sub)micrometric patches intensely labelled by BODIPY^{505}-SM and -GlcCer at the free surface of living erythrocytes cannot reflect local concentrations of an homogenously labelled membrane due to structural features, but represent domains of lipid enrichment at the outer PM leaflet. Two complementary approaches supported the same conclusion for CHO cells. Firstly, double labelling using two different sphingolipid analogs, BODIPY^{505}-SM and a BODIPY^{589}-glycosphingolipid, showed almost complete segregation. If these distinct lipids had been homogenously distributed along the PM, a parallel enrichment leading to co-localization should be expected if patches were simply revealing projecting surface features. Secondly, BODIPY-SM domains could be segregated from cortical actin, both spatially and functionally. Thus, also in cells with irregular cell surface, (sub)micrometric patches did not relate to membrane projections supported by cortical actin microfilaments. These features of SM micrometric domains thus differ from the properties of PIP_2 patches at the inner PM leaflet, which reflect its local enrichment by topological structuring of the cell surface. Indeed, PIP_2 patches: (i) co-localize with membrane ruffles and microvilli where they associate with F-actin; (ii) are enriched to a lesser extent (~2–3-fold over the rest of the PM) as compared with BODIPY-SM (~4–8-fold); and (iii) disappear upon hypotonic cell swelling [38].

We also ruled out the possibility that insertion of amphipathic compounds such as fluorescent SLs (which prefer the outer leaflet as reflected by their sensitivity to surface back-exchange with BSA) would expand the outer leaflet relative to the inner one, triggering the protrusions of "echinocytic" spicules [58]. For instance, we found no echinocyte deformation by scanning electron microscopy when erythrocytes were immobilized on poly-L-lysine and labelled with BODIPY-SM. At the opposite, when erythrocytes were directly put on naked glass, most cells showed strong echinocyte deformation: remarkably, no BODIPY-SM domain could be observed in these grossly deformed cells, but were obvious in the few preserved erythrocytes (data not shown).

4.5. Limitations of BODIPY-SM as a surrogate tracer of endogenous SM, but indirect evidence for micrometric SM domains as a L_o-phase

To what extent do BODIPY-SM PM domains reflect a similar organization for endogenous SM is still open to discussion. Although BODIPY^{505}-SM has been widely used to follow membrane trafficking, there is no question that, due to the fluorophore substitution to be inserted deep within the outer membrane leaflet, chain-labelled fluorescent sphingolipid "analogs" are not equivalent to natural SM. Indeed, they show quantitative differences such as higher PM insertion efficacy and lesser partitioning into DRMs. It thus remains necessary to evaluate their validity as *bona fide* qualitative tracers of endogenous SM for each type of experiment. Nevertheless, fluorescent SM analogs have already been reported by another group to exhibit striking qualitative similarities with endogenous sphingolipids, such as SM- and cholesterol dependence for confinement to distinct cell surface domains [8], as for the micrometric domains visualized by confocal microscopy in this report. In addition, partition of membrane lipid fluorescent analogs into L_o-phase cannot be explained by the grafted fluorophore alone, but clearly depended on host membrane composition. Indeed, while most membrane lipid tracers, including C_{12}-BODIPY-SM and DiIC18, strongly partition in the L_d-phase in elementary membrane model systems such as GUVs [55], C_6-NBD-SM (but not C_{12}-NBD-PC) preferentially partitions into the L_o-like phase in GPMVs [74]. Moreover, the same differences between GUVs and GPMVs have been reported for the partitioning of GPI-anchored protein, Thy-1, labelled by a MAb at significant distance outside the membrane bilayer [74]. A higher compactness of L_o-phases in synthetic lipid mixtures such as in GUVs than in GPMVs could explain these partition differences [74]. Since GPMVs more accurately reflect the properties of the composite natural PM, it seems reasonable to suggest that NBD-SM and BODIPY-SM probes used in this study also preferentially partition in the L_o-phase in living cells.

We have further provided several lines of evidence that BODIPY-SM is an acceptable qualitative surrogate of natural SM for the purpose of our study. Firstly, switching the very different BODIPY^{505} and NBD fluorophores of SM derivatives did not appreciably influence the formation of membrane domains visible by confocal microscopy nor the lateral mobility by FRAP. Moreover, BODIPY^{505}- and BODIPY^{589}-derivatives of SM showed perfect co-localization. Secondly, BODIPY^{505}-SM spontaneously clustered into ordered PM domains when added at high concentrations, as reflected by the "excimer" spectral shift, thereby mimicking the well-known self-clustering of natural SLs. Thirdly, our analysis revealed distinct temperature-dependence of domain formation and/or maintenance for BODIPY^{505}-SM and -GlcCer, with the same ranking as corresponding endogenous SLs Tm values [51,52]. This observation is consistent with the hypothesis that SL analogs also associate with L_o-lipid domains, like natural SLs. Fourthly and most interestingly, endogenous SM depletion by sphingomyelinase or fumonisin B1 strongly impaired formation and/or maintenance of BODIPY^{505}-SM domains, as observed by confocal microscopy. In addition, sphingomyelinase affected its lateral diffusion properties as measured by FRAP, whereas in FB1-treated cells, only C_6-SM repletion could reach the mobile fraction of untreated cells in small fields. As a related functional evidence, treatment with another short-chain SL, C_8-lactosylceramide, was reported to specifically trigger caveolar-dependent endocytosis as compared with other endocytic mechanisms [69]. Taken together, these various lines of evidence support the contention that BODIPY-SM is a reasonable qualitative surrogate tracer of endogenous SM and the proposal that BODIPY-SM patches may reflect constitutive preexisting micrometric SM domains at the outer PM leaflet.

4.6. How is the shape of BODIPY-SM micrometric PM domains defined by liquid-phase coexistence?

Upon lowering temperature of GUVs made of PC, SM and cholesterol, a separation into coexisting liquid-phases can be observed at 37 °C and increases below 25 °C [75]. A phase separation at the lower temperature is exactly what we observed at the erythrocyte membrane for BODIPY-SM domains, whose number and occupied surface increased as temperature decreased from 37 °C to 20 °C. Moreover, this observation is in reasonable agreement with the reported major phase transition at ~34 °C for the SL-rich outer leaflet of the erythrocyte membrane [30]. The strong increase of BODIPY-GlcCer domain number and total surface we observed when temperature was raised from 20 °C to 37 °C could be explained by higher Tm for natural cerebrosides, ~55 °C [51], than for most natural SMs, close to 37 °C [52]. Whether Tm values are comparable for BODIPY^{505}-SM and -GSLs remains to be measured. Together with the effects of membrane tension and cholesterol modulation on the size of BODIPY^{505}-SM patches, the major opposite role of temperature on BODIPY^{505}-SM and -GlcCer domain formation at erythrocytes, combined with their clear segregation in CHO cells at 37 °C, strongly suggests distinct phase behaviour, i.e. phase coexistence under physiological conditions. Combination with the round shape of BODIPY-SM and -GlcCer domains in erythrocytes leads us to further speculate that liquid-phase coexistence could provide the physical basis for endogenous SM organization in living cells.

4.7. How is the size of BODIPY-SM micrometric domains simultaneously controlled by membrane tension and cholesterol?

Since the formation and/or maintenance of BODIPY-SM micrometric domains in living cells could be explained by liquid-phase coexistence, which is a temperature-dependent process, and since line tension between two phases of GPMVs approaches zero as temperature is increased to the transition [50], it seems reasonable to suggest that the size of SM domains is controlled by membrane tension, which can be increased independently by hypotonicity and by cholesterol depletion [76]. In good agreement with this proposal, we observed that both exposure of living erythrocytes to hypotonicity and treatment of CHO cells with mβCD led to coalescence of BODIPY-SM micrometric domains.

4.8. Coexistence of distinct micrometric domains and their functional relevance

Since micrometric domains have been independently reported for PC and LacCer fluorescent analogs [34,35], and since lateral diffusion properties are clearly distinct between D-*e*-LacCer and SM, we postulate that several types of micrometric domains coexist at the cell surface. Assuming a representative behaviour of the surfaces we analyzed, area estimations indicate that BODIPY-SM domains account from 7% of the erythrocyte surface at 20 °C to ~20% in CHO cells at 10 °C. Incidentally, the respective ~8-fold and ~4-fold enrichment in these micrometric domains roughly indicates that about half of total SM at the outer leaflet would be clustered in these domains, which is a considerable pool. Probably more important, the relatively small area occupied by BODIPY-SM micrometric domains leaves ample room for

additional distinct domain(s), that could be enriched in GSLs, such as LacCer as documented for BODIPY-D-*e*-LacCer, or PC. In this paper, we already noted that SM and GSLs diffusion properties in FRAP were differentially affected by field size and that BODIPY^{589}-SM largely segregated from BODIPY^{505}-D-*e*-LacCer by confocal imaging. Incidentally, we also observed that micrometric domains of the other L_o-reporter, GPI-GFP, did not co-localize with BODIPY-SM, but did so with a D-*e*-LacCer analog (D'Auria et al, in preparation). Moreover, whereas replenishment of FB1-treated cells by C_6-SM largely relaxed the restriction to BODIPY-SM lateral mobility in large fields, replenishment by a GSL, GM3, had opposite effect. These various lines of evidence predict for distinct SM and GSL domains. A comprehensive analysis based on multiple labelling, detailed FRAP measurements and several controlled perturbations, being finalised in our laboratory, fully supports the coexistence of biochemically and functionally distinct micrometric PM lipid domains (D'auria et al., in preparation).

Their significance remains, however, essentially unknown. Conceivably, micrometric lipid modular organization would favor fluidity and large-scale selective lipid transport, as required during rapid cell movement. In addition, as also implied for the nanometric lipid rafts, micrometric domains may play a role in signalling, membrane curvature and cell polarity. At the inner membrane leaflet, highly dynamic micrometric PIP_2 domains develop with the phagocytic cup, where they favor signalling, actin remodelling and membrane curvature [77]. In budding yeasts, concentration of phosphatidylethanolamine at polarized ends is implicated in single cell polarity [78]. During epithelial sheet polarization, differential enrichment of PIP_2 at the apical surface and PIP_3 at the basolateral surface is also a crucial event [79,80]. As key questions (and suggested fields for future investigations), it remains to clarify (i) to what extent do nanometric rafts undergo regulated coalescence into micrometric domains under various appropriate conditions, as already suggested for the immunological synapse [15] and for platelet activation [31,32]; (ii) whether non-raft lipids also form micrometric domains, coexisting with L_o-phases; and (iii) the relevance of these diverse domains to various aspects of cell physiology.

Acknowledgements

This work was supported by grants from UCL, F.R.S./FNRS, Région wallonne, Région bruxelloise, Loterie Nationale, ARC and IUAP (Belgium), EuReGene and EuNephron (EU). D.T. was Research Associate at the FNRS/FRIA, at which L. D'Auria and J.C. Monbaliu were Research fellows. We are particularly grateful to Dr. R. Pagano (Mayo, Rochester, MN, USA) for precious samples of BODIPY-D-*e*-LacCer, extensive discussions and excellent advices, Dr. J. Marchand (CHOM, UCL) for generous interest and sustained help in the synthesis and characterization of BODIPY analogs, Drs D. Vertommen and V. Stroobant (UCL and de Duve Institute) for mass spectrometry, as well as Drs K. Simons (MPI, Dresden, Germany) and P. Zimmermann (KUL, Leuven, Belgium) for sharing GL-GPI-GFP and actin-YFP plasmids. We also thank Mrs M. Leruth and T. Lac and Mr. Y. Marchand for illustration and typing assistance.

Appendix A. Supplementary data

Supplementary data associated with this article can be found, in the online version, at doi:10.1016/j.bbamem.2010.01.021.

References

[1] E. Lauwers, G. Grossmann, B. Andre, Evidence for coupled biogenesis of yeast Gap1 permease and sphingolipids: essential role in transport activity and normal control by ubiquitination, Mol. Biol. Cell 18 (2007) 3068–3080.
[2] Y.A. Hannun, L.M. Obeid, Principles of bioactive lipid signalling: lessons from sphingolipids, Nat. Rev. Mol. Cell Biol. 9 (2008) 139–150.
[3] S.J. Singer, G.L. Nicolson, The fluid mosaic model of the structure of cell membranes, Science 175 (1972) 720–731.
[4] K. Simons, E. Ikonen, Functional rafts in cell membranes, Nature 387 (1997) 569–572.
[5] M. Edidin, The state of lipid rafts: from model membranes to cells, Annu. Rev. Biophys. Biomol. Struct. 32 (2003) 257–283.
[6] D.A. Brown, E. London, Functions of lipid rafts in biological membranes, Annu. Rev. Cell Dev. Biol. 14 (1998) 111–136.
[7] P. de Diesbach, T. Medts, S. Carpentier, L. D'Auria, P. Van Der Smissen, A. Platek, M. Mettlen, A. Caplanusi, M.F. van den Hove, D. Tyteca, P.J. Courtoy, Differential subcellular membrane recruitment of Src may specify its downstream signalling, Exp. Cell Res. 314 (2008) 1465–1479.
[8] P.F. Lenne, L. Wawrezinieck, F. Conchonaud, O. Wurtz, A. Boned, X.J. Guo, H. Rigneault, H.T. He, D. Marguet, Dynamic molecular confinement in the plasma membrane by microdomains and the cytoskeleton meshwork, EMBO J. 25 (2006) 3245–3256.
[9] D.E. Saslowsky, J. Lawrence, X. Ren, D.A. Brown, R.M. Henderson, J.M. Edwardson, Placental alkaline phosphatase is efficiently targeted to rafts in supported lipid bilayers, J. Biol. Chem. 277 (2002) 26966–26970.
[10] C. Eggeling, C. Ringemann, R. Medda, G. Schwarzmann, K. Sandhoff, S. Polyakova, V.N. Belov, B. Hein, C. von Middendorff, A. Schonle, S.W. Hell, Direct observation of the nanoscale dynamics of membrane lipids in a living cell, Nature 457 (2009) 1159–1162.
[11] P.W. Janes, S.C. Ley, A.I. Magee, Aggregation of lipid rafts accompanies signaling via the T cell antigen receptor, J. Cell Biol. 147 (1999) 447–461.
[12] P.F. Almeida, A. Pokorny, A. Hinderliter, Thermodynamics of membrane domains, Biochim. Biophys. Acta 1720 (2005) 1–13.
[13] P.A. Janmey, P.K. Kinnunen, Biophysical properties of lipids and dynamic membranes, Trends Cell Biol. 16 (2006) 538–546.
[14] S. Mukherjee, F.R. Maxfield, Membrane domains, Annu. Rev. Cell Dev. Biol. 20 (2004) 839–866.
[15] R. Tavano, G. Gri, B. Molon, B. Marinari, C.E. Rudd, L. Tuosto, A. Viola, CD28 and lipid rafts coordinate recruitment of Lck to the immunological synapse of human T lymphocytes, J. Immunol. 173 (2004) 5392–5397.
[16] S. Mayor, R.E. Pagano, Pathways of clathrin-independent endocytosis, Nat. Rev. Mol. Cell Biol. 8 (2007) 603–612.
[17] E. Lauwers, B. Andre, Association of yeast transporters with detergent-resistant membranes correlates with their cell-surface location, Traffic 7 (2006) 1045–1059.
[18] L.J. Pike, Rafts defined: a report on the Keystone Symposium on Lipid Rafts and Cell Function, J. Lipid Res. 47 (2006) 1597–1598.
[19] L.J. Pike, The challenge of lipid rafts, J. Lipid Res. 50 (2009) S323–S328 Suppl.
[20] L.A. Bagatolli, To see or not to see: lateral organization of biological membranes and fluorescence microscopy, Biochim. Biophys. Acta 1758 (2006) 1541–1556.
[21] G. van Meer, D.R. Voelker, G.W. Feigenson, Membrane lipids: where they are and how they behave, Nat. Rev. Mol. Cell Biol. 9 (2008) 112–124.
[22] C. Dietrich, Z.N. Volovyk, M. Levi, N.L. Thompson, K. Jacobson, Partitioning of Thy-1, GM1, and cross-linked phospholipid analogs into lipid rafts reconstituted in supported model membrane monolayers, Proc. Natl. Acad. Sci. U. S. A. 98 (2001) 10642–10647.
[23] N. Kahya, D. Scherfeld, K. Bacia, B. Poolman, P. Schwille, Probing lipid mobility of raft-exhibiting model membranes by fluorescence correlation spectroscopy, J. Biol. Chem. 278 (2003) 28109–28115.
[24] T. Baumgart, A.T. Hammond, P. Sengupta, S.T. Hess, D.A. Holowka, B.A. Baird, W.W. Webb, Large-scale fluid/fluid phase separation of proteins and lipids in giant plasma membrane vesicles, Proc. Natl. Acad. Sci. U. S. A. 104 (2007) 3165–3170.
[25] W. Rodgers, M. Glaser, Characterization of lipid domains in erythrocyte membranes, Proc. Natl. Acad. Sci. U. S. A. 88 (1991) 1364–1368.
[26] L.R. Montes, D.J. Lopez, J. Sot, L.A. Bagatolli, M.J. Stonehouse, M.L. Vasil, B.X. Wu, Y.A. Hannun, F.M. Goni, A. Alonso, Ceramide-enriched membrane domains in red blood cells and the mechanism of sphingomyelinase-induced hot–cold hemolysis, Biochemistry 47 (2008) 11222–11230.
[27] M. Hao, S. Mukherjee, F.R. Maxfield, Cholesterol depletion induces large scale domain segregation in living cell membranes, Proc. Natl. Acad. Sci. U. S. A. 98 (2001) 13072–13077.
[28] A.L. Heiner, E. Gibbons, J.L. Fairbourn, L.J. Gonzalez, C.O. McLemore, T.J. Brueseke, A.M. Judd, J.D. Bell, Effects of cholesterol on physical properties of human erythrocyte membranes: impact on susceptibility to hydrolysis by secretory phospholipase A2, Biophys. J. 94 (2008) 3084–3093.
[29] B.M. Stott, M.P. Vu, C.O. McLemore, M.S. Lund, E. Gibbons, T.J. Brueseke, H.A. Wilson-Ashworth, J.D. Bell, Use of fluorescence to determine the effects of cholesterol on lipid behavior in sphingomyelin liposomes and erythrocyte membranes, J. Lipid Res. 49 (2008) 1202–1215.
[30] W.F. Wolkers, L.M. Crowe, N.M. Tsvetkova, F. Tablin, J.H. Crowe, In situ assessment of erythrocyte membrane properties during cold storage, Mol. Membr. Biol. 19 (2002) 59–65.
[31] K. Gousset, W.F. Wolkers, N.M. Tsvetkova, A.E. Oliver, C.L. Field, N.J. Walker, J.H. Crowe, F. Tablin, Evidence for a physiological role for membrane rafts in human platelets, J. Cell. Physiol. 190 (2002) 117–128.
[32] R. Bali, L. Savino, D.A. Ramirez, N.M. Tsvetkova, L. Bagatolli, F. Tablin, J.H. Crowe, C. Leidy, Macroscopic domain formation during cooling in the platelet plasma membrane: an issue of low cholesterol content, Biochim. Biophys. Acta 1788 (2009) 1229–1237.

[33] K. Gaus, E. Gratton, E.P. Kable, A.S. Jones, I. Gelissen, L. Kritharides, W. Jessup, Visualizing lipid structure and raft domains in living cells with two-photon microscopy, Proc. Natl. Acad. Sci. U. S. A. 100 (2003) 15554–15559.
[34] R.D. Singh, Y. Liu, C.L. Wheatley, E.L. Holicky, A. Makino, D.L. Marks, T. Kobayashi, G. Subramaniam, R. Bittman, R.E. Pagano, Caveolar endocytosis and microdomain association of a glycosphingolipid analog is dependent on its sphingosine stereochemistry, J. Biol. Chem. 281 (2006) 30660–30668.
[35] E. Yechiel, M. Edidin, Micrometer-scale domains in fibroblast plasma membranes, J. Cell Biol. 105 (1987) 755–760.
[36] D. Meder, M.J. Moreno, P. Verkade, W.L. Vaz, K. Simons, Phase coexistence and connectivity in the apical membrane of polarized epithelial cells, Proc. Natl. Acad. Sci. U. S. A. 103 (2006) 329–334.
[37] T. Harder, P. Scheiffele, P. Verkade, K. Simons, Lipid domain structure of the plasma membrane revealed by patching of membrane components, J. Cell Biol. 141 (1998) 929–942.
[38] J. van Rheenen, K. Jalink, Agonist-induced PIP(2) hydrolysis inhibits cortical actin dynamics: regulation at a global but not at a micrometer scale, Mol. Biol. Cell 13 (2002) 3257–3267.
[39] D. Wustner, Plasma membrane sterol distribution resembles the surface topography of living cells, Mol. Biol. Cell 18 (2007) 211–228.
[40] G. Schwarzmann, K. Sandhoff, Lysogangliosides: synthesis and use in preparing labeled gangliosides, Methods Enzymol. 138 (1987) 319–341.
[41] E.G. Bligh, W.J. Dyer, A rapid method of total lipid extraction and purification, Can. J. Biochem. Physiol. 37 (1959) 911–917.
[42] Z.J. Cheng, R.D. Singh, D.K. Sharma, E.L. Holicky, K. Hanada, D.L. Marks, R.E. Pagano, Distinct mechanisms of clathrin-independent endocytosis have unique sphingolipid requirements, Mol. Biol. Cell 17 (2006) 3197–3210.
[43] D. Tyteca, P. Van Der Smissen, M. Mettlen, F. Van Bambeke, P.M. Tulkens, M.P. Mingeot-Leclercq, P.J. Courtoy, Azithromycin, a lysosomotropic antibiotic, has distinct effects on fluid-phase and receptor-mediated endocytosis, but does not impair phagocytosis in J774 macrophages, Exp. Cell Res. 281 (2002) 86–100.
[44] P. Cupers, A. Veithen, A. Kiss, P. Baudhuin, P.J. Courtoy, Clathrin polymerization is not required for bulk-phase endocytosis in rat fetal fibroblasts, J. Cell Biol. 127 (1994) 725–735.
[45] O.C. Martin, R.E. Pagano, Internalization and sorting of a fluorescent analogue of glucosylceramide to the Golgi apparatus of human skin fibroblasts: utilization of endocytic and nonendocytic transport mechanisms, J. Cell Biol. 125 (1994) 769–781.
[46] D. Tyteca, S.C. van Ijzendoorn, D. Hoekstra, Calmodulin modulates hepatic membrane polarity by protein kinase C-sensitive steps in the basolateral endocytic pathway, Exp. Cell Res. 310 (2005) 293–302.
[47] S.C. van IJzendoorn, M.M. Zegers, J.W. Kok, D. Hoekstra, Segregation of glucosylceramide and sphingomyelin occurs in the apical to basolateral transcytotic route in HepG2 cells, J. Cell Biol. 137 (1997) 347–357.
[48] V. Puri, R. Watanabe, R.D. Singh, M. Dominguez, J.C. Brown, C.L. Wheatley, D.L. Marks, R.E. Pagano, Clathrin-dependent and -independent internalization of plasma membrane sphingolipids initiates two Golgi targeting pathways, J. Cell Biol. 154 (2001) 535–547.
[49] P.F. Devaux, R. Morris, Transmembrane asymmetry and lateral domains in biological membranes, Traffic 5 (2004) 241–246.
[50] S.L. Veatch, P. Cicuta, P. Sengupta, A. Honerkamp-Smith, D. Holowka, B. Baird, Critical fluctuations in plasma membrane vesicles, ACS Chem. Biol. 3 (2008) 287–293.
[51] A.W. Clowes, R.J. Cherry, D. Chapman, Physical properties of lecithin-cerebroside bilayers, Biochim. Biophys. Acta 249 (1971) 301–317.
[52] B. Ramstedt, J.P. Slotte, Membrane properties of sphingomyelins, FEBS Lett. 531 (2002) 33–37.
[53] D. Illinger, P. Poindron, P. Fonteneau, M. Modollel, J.G. Kuhry, Internalization of the lipophilic fluorescent probe trimethylamino-diphenylhexatriene follows the endocytosis and recycling of the plasma membrane in cells, Biochim. Biophys. Acta 1030 (1990) 73–81.
[54] D. Illinger, P. Poindron, J.G. Kuhry, Fluid phase endocytosis investigated by fluorescence with trimethylamino-diphenylhexatriene in L929 cells; the influence of temperature and of cytoskeleton depolymerizing drugs, Biol. Cell 73 (1991) 131–138.
[55] T. Baumgart, G. Hunt, E.R. Farkas, W.W. Webb, G.W. Feigenson, Fluorescence probe partitioning between Lo/Ld phases in lipid membranes, Biochim. Biophys. Acta 1768 (2007) 2182–2194.
[56] K. Hanada, T. Hara, M. Fukasawa, A. Yamaji, M. Umeda, M. Nishijima, Mammalian cell mutants resistant to a sphingomyelin-directed cytolysin. Genetic and biochemical evidence for complex formation of the LCB1 protein with the LCB2 protein for serine palmitoyltransferase, J. Biol. Chem. 273 (1998) 33787–33794.
[57] J.F. Bouhours, D. Bouhours, J. Delaunay, Abnormal fatty acid composition of erythrocyte glycosphingolipids in congenital dyserythropoietic anemia type II, J. Lipid Res. 26 (1985) 435–441.
[58] H.W.G. Lim, M. Wortis, R. Mukhopadhyay, Stomatocyte–discocyte–echinocyte sequence of the human red blood cell: evidence for the bilayer-couple hypothesis from membrane mechanics, Proc. Natl. Acad. Sci. U. S. A. 99 (2002) 16766–16769.
[59] T.C. Walther, J.H. Brickner, P.S. Aguilar, S. Bernales, C. Pantoja, P. Walter, Eisosomes mark static sites of endocytosis, Nature 439 (2006) 998–1003.
[60] M. Hao, F.R. Maxfield, Characterization of rapid membrane internalization and recycling, J. Biol. Chem. 275 (2000) 15279–15286.
[61] R.E. Pagano, O.C. Martin, H.C. Kang, R.P. Haugland, A novel fluorescent ceramide analogue for studying membrane traffic in animal cells: accumulation at the Golgi apparatus results in altered spectral properties of the sphingolipid precursor, J. Cell Biol. 113 (1991) 1267–1279.
[62] X. Zha, L.M. Pierini, P.L. Leopold, P.J. Skiba, I. Tabas, F.R. Maxfield, Sphingomyelinase treatment induces ATP-independent endocytosis, J. Cell Biol. 140 (1998) 39–47.
[63] N.C. Hait, C.A. Oskeritzian, S.W. Paugh, S. Milstien, S. Spiegel, Sphingosine kinases, sphingosine 1-phosphate, apoptosis and diseases, Biochim. Biophys. Acta 1758 (2006) 2016–2026.
[64] A.K. Kenworthy, B.J. Nichols, C.L. Remmert, G.M. Hendrix, M. Kumar, J. Zimmerberg, J. Lippincott-Schwartz, Dynamics of putative raft-associated proteins at the cell surface, J. Cell Biol. 165 (2004) 735–746.
[65] D. Tyteca, A. Schanck, Y.F. Dufrene, M. Deleu, P.J. Courtoy, P.M. Tulkens, M.P. Mingeot-Leclercq, The macrolide antibiotic azithromycin interacts with lipids and affects membrane organization and fluidity: studies on Langmuir–Blodgett monolayers, liposomes and J774 macrophages, J. Membr. Biol. 192 (2003) 203–215.
[66] J.W. Kok, M. ter Beest, G. Scherphof, D. Hoekstra, A non-exchangeable fluorescent phospholipid analog as a membrane traffic marker of the endocytic pathway, Eur. J. Cell Biol. 53 (1990) 173–184.
[67] K.E. Magnusson, M. Gustafsson, K. Holmgren, B. Johansson, Small intestinal differentiation in human colon carcinoma HT29 cells has distinct effects on the lateral diffusion of lipids (ganglioside GM1) and proteins (HLA class 1, HLA class 2, and neoplastic epithelial antigens) in the apical cell membrane, J. Cell. Physiol. 143 (1990) 381–390.
[68] K. Bacia, D. Scherfeld, N. Kahya, P. Schwille, Fluorescence correlation spectroscopy relates rafts in model and native membranes, Biophys. J. 87 (2004) 1034–1043.
[69] D.K. Sharma, J.C. Brown, A. Choudhury, T.E. Peterson, E. Holicky, D.L. Marks, R. Simari, R.G. Parton, R.E. Pagano, Selective stimulation of caveolar endocytosis by glycosphingolipids and cholesterol, Mol. Biol. Cell 15 (2004) 3114–3122.
[70] M. Vrljic, S.Y. Nishimura, W.E. Moerner, H.M. McConnell, Cholesterol depletion suppresses the translational diffusion of class II major histocompatibility complex proteins in the plasma membrane, Biophys. J. 88 (2005) 334–347.
[71] H. Raghuraman, A. Chattopadhyay, Interaction of melittin with membrane cholesterol: a fluorescence approach, Biophys. J. 87 (2004) 2419–2432.
[72] V. Shahedi, G. Oradd, G. Lindblom, Domain-formation in DOPC/SM bilayers studied by pfg-NMR: effect of sterol structure, Biophys. J. 91 (2006) 2501–2507.
[73] J. Zhao, J. Wu, H. Shao, F. Kong, N. Jain, G. Hunt, G. Feigenson, Phase studies of model biomembranes: macroscopic coexistence of Lalpha + Lbeta, with light-induced coexistence of Lalpha + Lo phases, Biochim. Biophys. Acta 1768 (2007) 2777–2786.
[74] P. Sengupta, A. Hammond, D. Holowka, B. Baird, Structural determinants for partitioning of lipids and proteins between coexisting fluid phases in giant plasma membrane vesicles, Biochim. Biophys. Acta 1778 (2008) 20–32.
[75] S.L. Veatch, S.L. Keller, Miscibility phase diagrams of giant vesicles containing sphingomyelin, Phys. Rev. Lett. 94 (2005) 148101.
[76] F.J. Byfield, H. Aranda-Espinoza, V.G. Romanenko, G.H. Rothblat, I. Levitan, Cholesterol depletion increases membrane stiffness of aortic endothelial cells, Biophys. J. 87 (2004) 3336–3343.
[77] R.J. Botelho, M. Teruel, R. Dierckman, R. Anderson, A. Wells, J.D. York, T. Meyer, S. Grinstein, Localized biphasic changes in phosphatidylinositol-4, 5-bisphosphate at sites of phagocytosis, J. Cell Biol. 151 (2000) 1353–1368.
[78] K. Iwamoto, S. Kobayashi, R. Fukuda, M. Umeda, T. Kobayashi, A. Ohta, Local exposure of phosphatidylethanolamine on the yeast plasma membrane is implicated in cell polarity, Genes Cells 9 (2004) 891–903.
[79] F. Martin-Belmonte, A. Gassama, A. Datta, W. Yu, U. Rescher, V. Gerke, K. Mostov, PTEN-mediated apical segregation of phosphoinositides controls epithelial morphogenesis through Cdc42, Cell 128 (2007) 383–397.
[80] A. Gassama-Diagne, W. Yu, M. ter Beest, F. Martin-Belmonte, A. Kierbel, J. Engel, K. Mostov, Phosphatidylinositol-3, 4, 5-trisphosphate regulates the formation of the basolateral plasma membrane in epithelial cells, Nat. Cell Biol. 8 (2006) 963–970.